Available online at www.sciencedirect.com
SCIENCE DIRECT®
Precambrian Research 122 (2003) 159–182
Precambrian Research
www.elsevier.com/locate/precamres

Structural evolution and $^{40}Ar/^{39}Ar$ dating of the Zanhuang metamorphic domain in the North China Craton: constraints on Paleoproterozoic tectonothermal overprinting

Y.J. Wang [a], W.M. Fan [a], Y. Zhang [b,*], F. Guo [a]

[a] *Guangzhou Institute of Geochemistry, Chinese Academy of Sciences, Guangzhou, 510640, China*
[b] *CSIRO Exploration and Mining, P.O. Box 1130, Bentley, WA 6102, Australia*

Received 12 January 2001; received in revised form 3 April 2002; accepted 18 April 2002

Abstract

The Zanhuang domain in the hinterland of the North China Craton, consists of Archaean, Paleoproterozoic, Mesoproterozoic and Palaeozoic rocks, and was previously considered a Mesozoic metamorphic core complex. Our reappraisal of regional structural history and mineral $^{40}Ar/^{39}Ar$ geochronology shows that the domain was subjected to a number of deformation events and had a heterogeneous uplift-cooling history during the Paleoproterozoic. Four primary deformation events have been recognized in the domain. The first event reflects the earliest deformation in the region, however, only closed and rootless folds are preserved. D_2 was dominated by WNW-ESE shortening and top-to-ESE thrusting in a collisional environment. D_3 was a divergent extensional and ductile shearing event, driven by the post-collisional extensional collapse and exhumation of the thickened crust in the domain. D_4 was characterized by localized ductile shearing with the development of three NNE-trending ductile shear zones. The $^{40}Ar/^{39}Ar$ plateau ages derived from the thermochronology analyses of the biotite concentrates from the metamorphic rocks are interpreted as cooling ages through biotite $^{40}Ar/^{39}Ar$ closure temperature (300 °C) and this allows us to constrain the timing of deformation events. In conjunction with the evidence from structural analyses and previous geochronological data, we conclude that 1870 and 1870–1826 Ma define the timing of D_1 and D_2 events, respectively, while 1826–1793 Ma represents the age of D_3. The last event (D_4) occurred at 1689–1633 Ma, as constrained by $^{40}Ar/^{39}Ar$ plateau ages of biotite concentrates from the mylonites within the ductile shear zones. These data, together with K-feldspar $^{40}Ar/^{39}Ar$ geochronology, allows us to depict the cooling history of the region during the Paleoproterozoic and Mesoproterozoic. It appears that the uplift-cooling rate varies temporally and spatially in the region.

Keywords: $^{40}Ar/^{39}Ar$ thermochronology; Paleoproterozoic; Uplifting; Zanhuang domain; North China Craton

1. Introduction

The Taihang Mountains belt is located in the hinterland of the North China Craton and is composed of the Zanhuang and Fuping domains (marked as ZH and FP in Fig. 1A). It represents a tectonic transition zone between the Eastern and Western blocks of the North China Craton, which have different tectonic architectures (e.g. Zhao et al., 1998, 1999a,b, 2000, 2001; Zhao, 2001; Guan, 1998; Guan et al., 2002). The tectonic evolution of the Zanhuang and Fuping metamorphic domains has long been debated. Several

* Corresponding author. Tel.: +61-8-64368626; fax: +61-8-64368555.
E-mail address: yanhua.zhang@csiro.au (Y. Zhang).

0301-9268/02/$ – see front matter.
PII: S0301-9268(02)00210-3

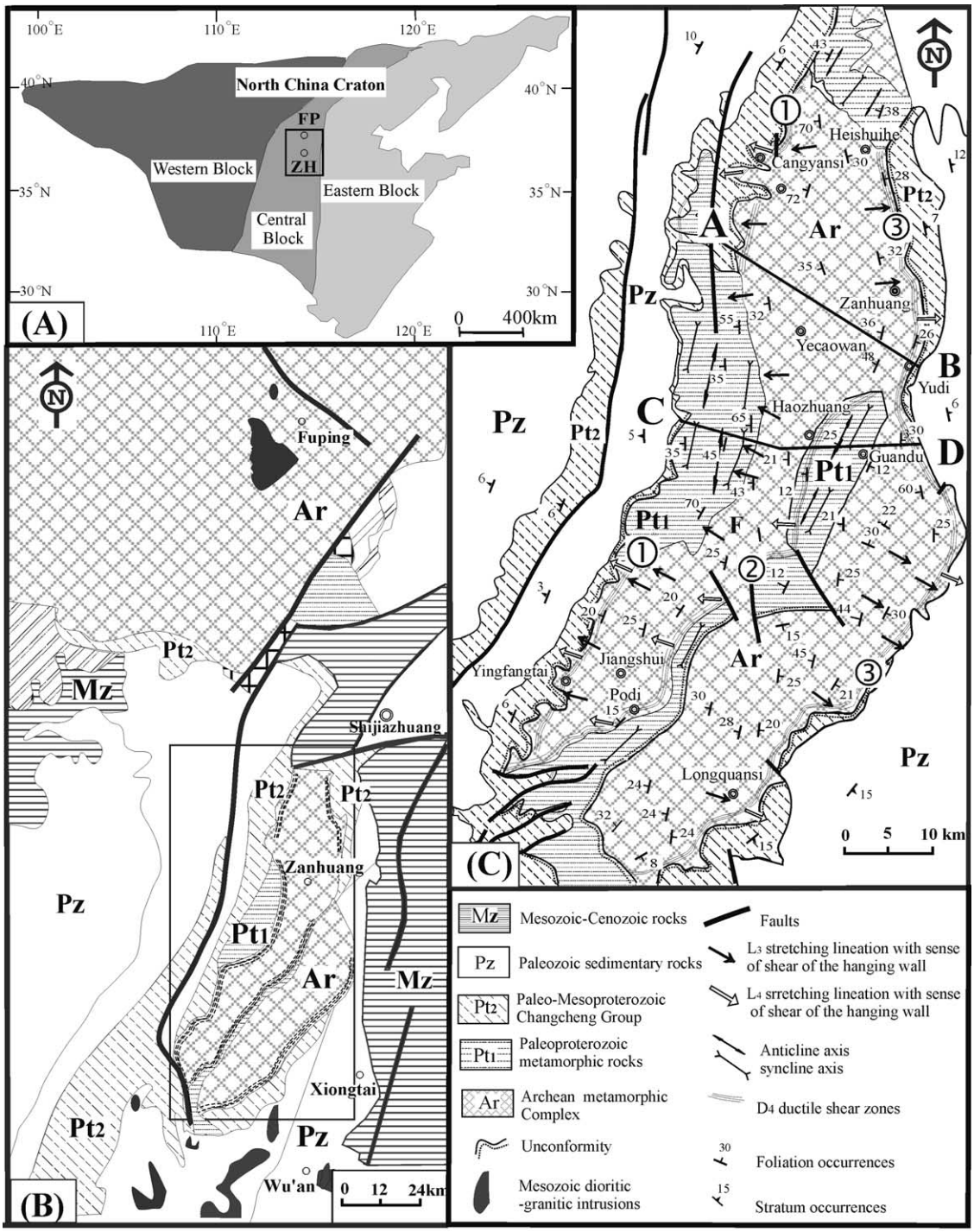

Fig. 1. (A) Tectonic location of the Zanhuang (ZH) and Fuping (FP) domains in the North China Craton. (B) and (C) Geological and structural maps of the Zanhuang domain, respectively (b is after Niu et al., 1994a,b). The locations of the Cangyansi–Yingfangtai, Podi–Haozhuang and Yudi–Heishuihe shear zones are indicated by ①, ② and ③, respectively, in (C).

different scenarios have been proposed. These include Archaean metamorphic dome (Ma, 1989), Precambrian compound fold dome (Zhang et al., 1983) and a late Archaean extensional deformation zone (Tang and Liu, 1997). Zhao et al. (1998, 1999a,b, 2000, 2001) and Zhao (2001) recently suggested that the basement of the North China Craton consists of the Eastern and Western Blocks joined together by the Central Block as a result of collision at ca. 1870 Ma (also see Wilde et al., 1997, 1998; Guan, 1998; Guan et al., 2002) (Fig. 1A). These authors believe that the Fuping and Zanhuang domains are important parts of the Central Block and represent Paleoproterozoic structures. Others (Ma and He, 1989; Niu et al., 1994a,b; Lei and Hu, 1994), however, considered that the Zanhuang and Fuping domains are Mesozoic metamorphic core complexes generated by intra-plate extensional deformation associated with rapid uplifting of possibly greater than 10 km. This was based on the presence of: (1) three major extensional NNE-trending ductile shear zones in the region which are approximately parallel to the boundaries of the domain; (2) Mesozoic granitic intrusions which occur in the areas near to the south margin of the Zanhuang domain (Fig. 1B).

It is widely accepted that metamorphic core complex structures such as those in the Basin and Range Province of western USA and the Wugongshan and Lushan regions of southeast China are typically extensional structures (e.g. Armstrong, 1982; Lister and Davis, 1989; Malavieille, 1997; Faure et al., 1996; Lin et al., 2000). They generally have domed footwalls capped by a ductile shear zone with a consistent normal movement sense and are commonly associated with syntectonic plutonism at the center of the dome (e.g. Malavieille, 1997; Faure et al., 1996; Lin et al., 2000). The Mesozoic extensional scenario for the Zanhuang and Fuping metamorphic domains (Niu et al., 1994a,b; Lei and Hu, 1994) seems to be quite compatible with this metamorphic core complex concept. However, there is a critical geochronological problem. The metamorphic basement with a crystallization age of 2400–2600 Ma in the Fuping domain appears to bear the signatures of the Lüliang tectonothermal event with an age of ca. 1850 Ma rather than that of the Mesozoic cooling events (e.g. Guan, 1998; Liu et al., 2000; Yu et al., 1997; Xu et al., 1995; Zhao et al., 1998, 2001). Intrusions are absent in the core area of the domains, although the Mesozoic granitic intrusions are exposed adjacent to the southern edge of the Zanhuang domain. This is in contrast with the observations reported for typical core complex models (e.g. Malavieille, 1997; Faure et al., 1996).

We recognize the fact that existing geochronological data are very sparse except for a few conventional K/Ar ages for the Zanhuang domain in the south Taihang Mountains (e.g. HBGMR, 1989). This, together with the lack of systematic kinematic studies, is the main reason for the uncertainties described above. To achieve a better understanding of the tectonic evolution of the region, extensive geochronological studies and systematic structural analysis are crucial. In this paper, we present the results of structural and mineral $^{40}Ar/^{39}Ar$ thermogeochronology studies of the Zanhuang domain with a focus on the structural evolution and tectonothermal overprinting history of the region. The Zanhuang domain was selected because it is situated far away from any known Mesozoic intra-continental active belt. In contrast, the Fuping domain in the North Taihang Mountains is close to Mesozoic Yanshanian reactivation structures and might be affected by Mesozoic tectonothermal events (e.g. Davis et al., 1998, 2001; Zheng et al., 1996).

2. Geological setting

The Zanhuang metamorphic domain is elongated and oriented in a NNE direction (Fig. 1C). The succession of rock units from base to top, and from core to margin includes Archaean high-grade metamorphic rocks, Paleoproterozoic metavolcanic rocks and metamorphic sandstone, the unmetamorphosed Paleo-mesoproterozoic Changcheng Group and Paleozoic–Mesozoic sedimentary rocks.

The Archaean high-grade metamorphic rocks in the domain, also termed the Zanhuang “Group” (e.g. HBGMR, 1989; Niu et al., 1994a) or Zanhuang Complex (e.g. Zhao et al., 2000, 2001), have a crystallization age of 2400–2600 Ma but unknown metamorphic ages. These rocks are generally considered the equivalent of the upper “subgroup” of the Fuping “Group” (or Fuping Complex) or of the Wutai “Group” (HBGMR, 1989; or Wutai Complex, see Zhao et al., 2000, 2001). It consists primarily of plagioclase amphibolite, biotite-plagioclase

gneiss, amphibole-plagioclase gneiss, leucogranulitite, quartzite, amphibole schist, quartz schist, marble, and migmatite (e.g. HBGMR, 1989; Niu et al., 1994a). Similar to the Wutai "Group", the Zanhuang "Group" was subjected to greenschist- to amphibolite-facies metamorphism. The temperature and pressure of the metamorphism, estimated from garnet-amphibole and biotite-garnet and related metamorphic reactions, are approximately 550–700 °C, 5–10 kbar for plagioclase-amphibolite and 400–620 °C, 4–8 kbar for mica-quartz schist (e.g. HBGMR, 1989). This is consistent with the *P–T* conditions (5.0–7.0 kbar and 550–650 °C) for amphibolite-facies metamorphism recorded in other domains in the Central Block of the North China Craton (e.g. Zhao et al., 2000, 2001; Zhang et al., 1994; Zhang, 1997).

The Paleoproterozoic metamorphic rocks (the Gantaohe and Honghe "Groups") uncomfortably overlie the Zanhuang "Group" and are composed of greenschist-facies mica-schist, sandstone, slate and metavolcanic rocks (HBGMR, 1989). These rocks are predominantly exposed in the western flank and axial zone of the domain (Fig. 1C). The temperature and pressure of the relevant metamorphism are approximately 350–500 °C and 3–7 kbar (HBGMR, 1989).

The Paleo-mesoproterozoic Changcheng Group consists of unmetamorphosed, gently dipping sandstones that uncomfortably overlie the metamorphic rocks described above, and was probably deposited from ca. 1700 Ma (Zhao et al., 2001; Li, 1992; Lu and Jin, 1993; Lu and Li, 1991). It is generally considered the lowest unit of the sedimentary cover in the North China Craton (e.g. HBGMR, 1989). On the eastern margin of the domain, the Paleoproterozoic Gantaohe and Honghe "Groups" are missing and the Changcheng Group or Paleozoic rocks directly overlie the Archaean metamorphic basement rocks (Fig. 1C).

There are no syn- and post-Paleoproterozoic granitic rocks outcropping within the Zanhuang domain except for the Mesozoic dioritic-granitic intrusions exposed in neighboring areas close to the south margin of the domain (Fig. 1B). The presence of Paleoproterozoic unmetamorphosed mafic dykes with a possible age of 1700–1800 Ma (50–200 m long and 3–10 m wide), however, is widespread in the basement of the domain (Qian and Chen, 1987; Zhai and Bian, 2000; Zhao et al., 2001). These dykes are predominantly NNE- and NW-trending, cutting directly across both Archaean and Paleoproterozoic rocks but covered by the Changcheng Group.

Three NNE trending ductile shear zones developed in the Zanhuang domain (Fig. 1C). From west to east, they are the Cangyansi–Yingfangtai shear zone, the Podi–Haozhuang shear zone and the Yudi–Heishuihe shear zone. Each shear zone has a combined length of >100 km and a width of 100–1000 m (Niu et al., 1994a,b; Lei, 1991), and is entirely hosted by the Archaean and Paleoproterozoic metamorphic rocks. Niu et al. (1994a,b) and Lei (1991) considered these shear zones to have formed during the Mesozoic but had no geochronological constraints to support their interpretation.

3. Structural analyses

Detailed structural work was carried out in the region to analyze the characteristics of folds, foliations, lineations, shear zones, faults and quartz *c*-axis fabrics. Special attention was given to overprinting relationships between structural elements wherever they could be confidently established. A multiple deformation history characterized by four deformation events is proposed herein for the Zanhuang domain (Table 1).

3.1. D_1 deformation

Evidence for the earliest deformation is represented by rootless and hook-like folds (F_1) of metamorphic rock bands and felsic veins in the Zanhuang "Group" high-grade metamorphic rocks (Figs. 2 and 3a). These small-scale tight folds are mainly preserved in the hinge zones of large-scale F_2. Elsewhere D_1 structures have been largely transposed by subsequent deformation events. As a result, the nature of the D_1 event is poorly understood.

3.2. D_2 deformation

D_2 was a compressive event and produced the dominant structural fabrics in the Zanhuang domain. D_2 structures include folds at various scales (F_2), a pervasive foliation (S_2) and some reverse faults that resulted in the duplication of the Zanhuang "Group" metamorphic rocks. F_2 folds in the Zanhuang "Group" are mostly at a clearly larger scale in comparison with

Table 1
Correlation between deformation events and structures

	Event			
	D_1	D_2	D_3	D_4
Folds	Rootless and hook-like folds (F_1)	Overturned and recumbent fold (F_2)	Post-S_2 foliation folds and open folds (F_3)	F_4 drag folds within the SZ_4 zones
Foliations		S_2 foliations dip toward WNW and are subparallel to F_2 fold axial planes	NNE-trending S_3 foliations dipping to WNW and ESE in the two flank, respectively	Mylonitic foliations dip gently to WNW or E in the different SZ_4
Lineations		Mineral lineations (L_2) with subparallel to F_2 fold axes or hinges	L_3 stretching lineations plunging toward WNW and ESE in the two flanks, respectively	E- or W-plunging stretching lineation (L_4) on S_4 foliation planes
Ductile shear			Ductile shearing (SZ_3) along "unconformity" between Ar and Pt_1 metamorphic rocks	Three NNE-trending ductile shear zones (SZ_4)
Faults		NE–NNE trending reverse faults, subparallel to F_2 fold axial planes	NNE-trending normal faults and the D_2-reactivated normal faults	Normal faults of various orientations
Overprinting relationship		F_1 rootless and hook-like folds are enclosed by S_2 foliations	Unmetamorphosed mafic dykes crosscut F_2 folds; D_3 faults and S_3 foliations cut S_2 foliations and F_2 folds; refolded S_2 in D_3	SZ_4 displaced F_2 folds, post-S_2 folds and S_3 foliation as well as unmetamorphic mafic dykes
Ages (Ma)	ca. 1870	ca. 1870–1826	ca. 1826–1793	1689–1633

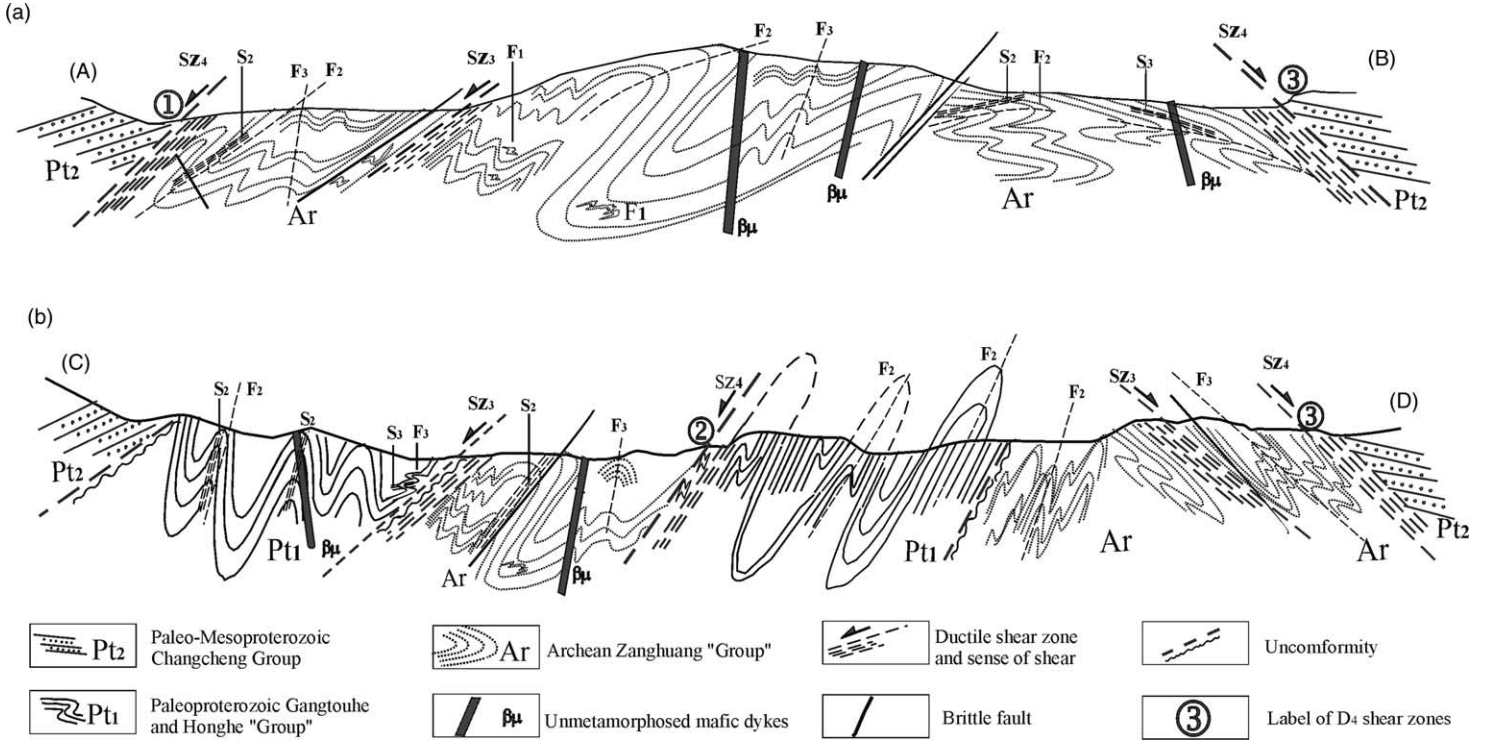

Fig. 2. Schematic cross-sections along profile lines A–B and C–D (see Fig. 1C for locations) in the Zanhuang domain. The locations of the NNE-trending Cangyansi–Yingfangtai, Podi–Haozhuang and Yudi–Heishuihe shear zones are indicated by ①, ② and ③, respectively. See text for more information.

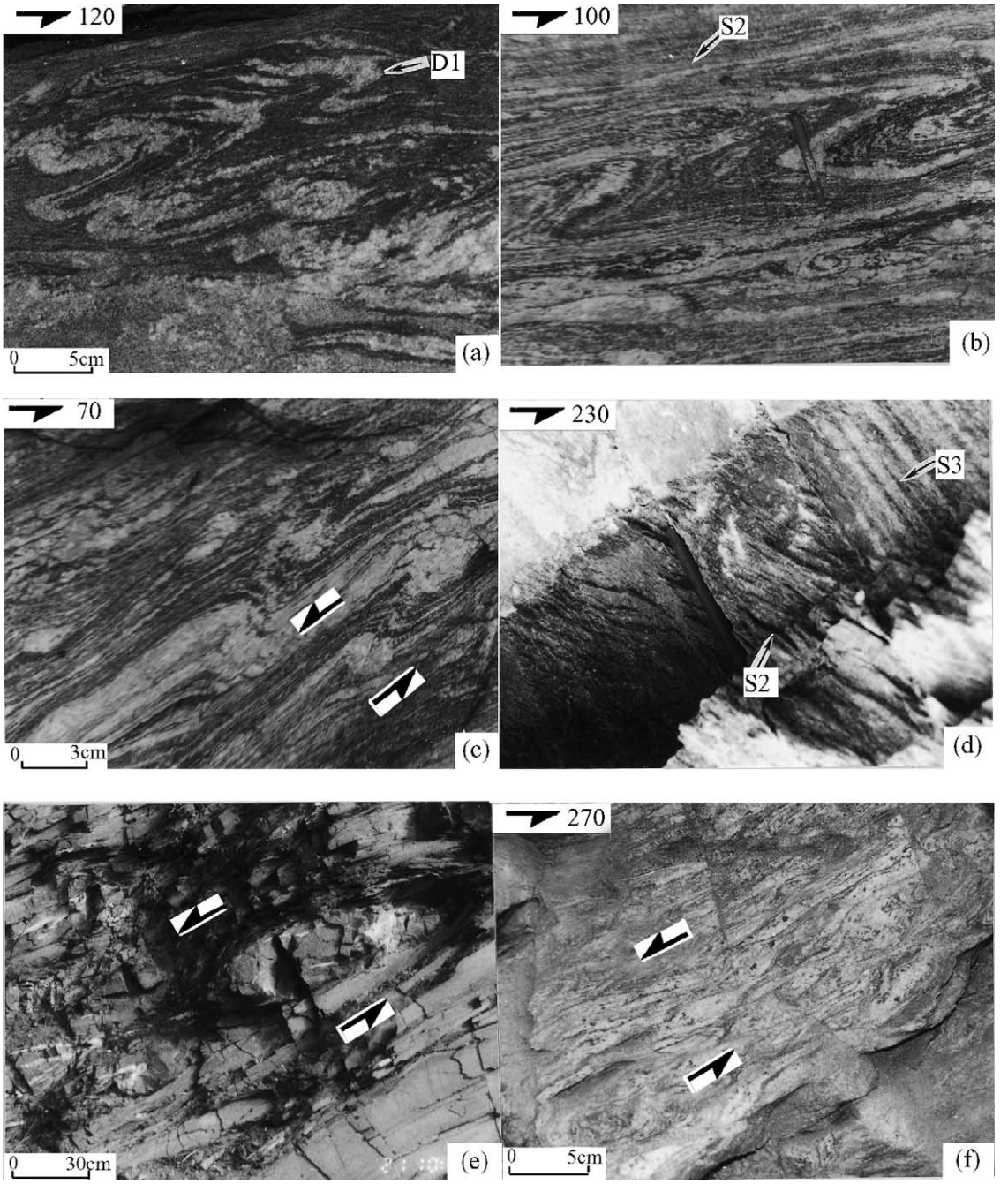

Fig. 3. Photographs showing structural features in the Zanhuang domain. (a) D_1 rootless and hook-like folds (F_1) in the Zanhuang "Group" metamorphic rocks (east of Jiangshui). (b) F_1 rootless and hook-like folds enclosed by S_2 foliations (west of Podi). (c) D_3 shear bands (SZ_3) and porphyroclasts in the upper part of the Zanhuang "Group" in the western flank of the Zanhuang domain, indicating a top-to-WNW shearing (south of Jiangshui). (d) An overprinting relationship of S_3 cutting S_2 (West of Yecaowang). (e) Outcrop-scale structural lenses in the Podi–Haozhuang shear zone, indicating a top-to-WNW shearing (east of Haozhuang). (f) Porphyroblasts and elongated quartz grains in the Heishuihe–Yudi shear zone, indicating a top-to-E shearing (east of Heishuihe). See text for more information.

F_1, ranging from a few meters to a few tens of kilometres in wavelength. They are represented by overturned and recumbent folds (Fig. 2). These folds generally exhibit markedly asymmetric geometries with significantly thickened hinge zones, and thinned and sheared limbs. It is noted that F_2 folds in the Archaean high grade metamorphic rocks are generally tighter than in the Paleoproterozoic greenschist rocks (Fig. 2). Numerous smaller scale, second order parasitic folds are also observed within larger scale F_2 folds in the Archaean rocks, with axial planes parallel to each other. The axial planes of F_2 folds generally dip to the WNW but locally to the ESE, and their hinges plunge shallowly to the NNE.

Axial planar foliations (S_2) were well developed throughout the Zanhuang "Group" metamorphic rocks (Figs. 1C and 2). They generally strike NNE and dip to the WNW, approximately parallel to F_2 fold axial planes. Anomalous S_2 foliation strike and dip orientations may also be observed in the region, most likely reflecting the influence of later faulting-related rotation. Within the S_2 foliation, mineral lineations (L_2) oriented parallel to F_2 fold axes or hinges are also observed, and they commonly consist of elongated minerals. S_2 foliations and L_2 lineations display quite different characteristics between the Archaean Zanhuang high-grade metamorphic rocks and the Paleoproterozoic metamorphic rocks. In the former, these fabrics are penetrative and are represented as pressure solution features and a strongly preferred alignment of moderate- and fine-grained muscovite, biotite, severely elongated quartz grains, and metamorphic hornblende (in amphibolitic rocks). In the latter, these fabrics are spaced and relatively weakly developed, and are primarily defined by discontinuous seams of opaque materials and a preferred alignment of slightly elongated quartz grains and minor metamorphic muscovite, biotite and chlorite. An overprinting relationship can be established between S_2 foliations and F_1 folds; F_1 rootless and hook-like folds are often entirely enclosed or truncated by S_2 foliations (Fig. 3b). This provides an important constraint on temporal relationship between D_1 and D_2 deformations.

D_2 faults commonly developed along the thinned limbs of the F_2 overturned folds (Fig. 2). These faults trend NE–NNE and dip to the NW–WNW, approximately parallel to F_2 fold axial planes and S_2 foliations. Displacement of lithological markers and the geometry of associated drag folds indicate a reverse movement on these faults during D_2 deformation.

The kinematics of D_2 deformation can be inferred from the structural observations described above. The structural features of F_2 folds (asymmetric geometry, axial plane trending and dipping), S_2 foliations (morphological features), and D_2 faults (reverse faulting) all point to a kinematic scenario with a WNW–ESE shortening and a ESE structural transport direction (top-to-ESE thrusting).

3.3. D_3 deformation

Field evidence for D_3 deformation includes the observation of mylonitic foliation (S_3), mineral stretching lineation (L_3), some post-D_2 folds (F_3) and low-angle normal faults.

S_3 mylonitic foliations and related L_3 lineations provided important information about D_3 event. These fabrics are represented by the development of mylonitic greenschist, mylonitic gneisses, protomylonites and quartz-feldspar mylonites along lithological boundaries, particularly along the regional "unconformity" contact between the Archaean and Paleoproterozoic metamorphic rocks (Fig. 2). S_3 foliations are pervasive and consist of muscovite, biotite, and elongated quartz grains, with L_3 stretched lineations defined by elongated and preferably oriented quartz and feldspar grains. Amphibole was also seen within S_3 foliations in the portions of the Archaean metamorphic rocks near the regional "unconformity" contact. The geometries of S_3 foliations and L_3 lineations exhibit clear differences between the western and the eastern flanks of the Zanhuang domain. In the western flank, S_3 foliations are NNE-trending and WNW-dipping, with L_3 lineations plunging toward the WNW direction. In contrast, S_3 foliations in the eastern flank are ESE-dipping, with L_3 lineations plunging toward the ESE direction (Fig. 1C). It needs to be mentioned that S_3 foliations usually dip more gently in comparison with S_2 foliations, though both have very similar trending orientations. An overprinting relationship of S_3 cutting S_2 can be observed (Fig. 3d) and this provides critical constraints on the relative timing sequence of D_3 event.

Microstructures associated with the S_3 mylonitic foliations indicate that ductile shearing was the dominant mode of deformation. Kinematic indicators

reflecting the local sense of shearing include mica fish, microscale shear bands, dynamically recrystallized quartz grains oblique to the foliations, S-C fabrics, asymmetrical boudins, δ- and σ-type porphyroclasts (Fig. 3c), small-scale and asymmetric folds (cf. Simpson and Schmid, 1983; Cobbold et al., 1987; Twiss and Moores, 1994). All these indicators suggest a divergent sense of shearing from the western to the eastern flanks across the region, that is, top-to-WNW extensional shearing in the western flank and top-to-ESE extensional shearing in the eastern flank. This deformation pattern is likely the result of a regional sideways extension divergent from the central zone of the domain, directly related to the uplift and collapse of the axial zone of the Zanhuang domain.

F_3 folds are characterized by folding of S_2 foliations and also by the development of some open folds (F_3). These folds generally occur at smaller scales in comparison with F_2 folds (Fig. 2). The development of some recumbent folds in the eastern flank of the Zanhuang domain could be attributed to the rotation of F_2 folds during D_3 top-to-ESE extensional shearing (Fig. 2). Some small-scale overturned folds (F_3) were also observed locally in the western flank (Fig. 2b) and they appear to reflect top-to-WNW extensional shearing there. NNE-trending normal faults developed during D_3 and there is also evidence that some D_2 faults were reactivated in a normal sense. The displacement patterns of these faults are consistent with the shearing movements reflected by other structures (e.g. S_3 foliations). Some of these faults offset S_2 cleavage and F_2 folds.

The quartz *c*-axis preferred orientations of Archaean and Paleoproterozoic metamorphic and mylonitic rocks have been measured using a universal stage (Fig. 4; cf. Simpson and Schmid, 1983; Cobbold et al., 1987). The patterns are consistent with the kinematics of D_3 deformation, as proposed by the structural analyses described above. For samples collected from the central zone of the Zanhuang domain or the localities far away from major shearing surfaces (99HXT-15, 99HXT-9, 99HXT-27, 99JX-32, 99HXT-36, 99JX-68, 99JX-65, 99JX-91 and 99JX-85), the derived fabric patterns show two maxima symmetrical about the shortening axis and stretching lineation orientation (Fig. 4). This reflects the coaxial deformation kinematics associated with broad regional extension (see Law, 1990; Twiss and Moores, 1994). However, for samples taken from localities near the "unconformity" contact where the maximum shearing occurred (99JX-38 and 99HXT-5), the quartz *c*-axis fabrics display point-maxima patterns asymmetrical with respect to the shortening axis and lineation orientations (Fig. 4). This is basically consistent with non-coaxial deformation associated with localized shearing at such structural localities (see Law, 1990; Twiss and Moores, 1994). The quartz *c*-axis fabrics patterns described above suggest that the basal ⟨a⟩ crystallographic planes were the dominant gliding system during D_3 deformation, which is the situation generally proposed for lower temperature or higher strain rate conditions (e.g. Twiss and Moores, 1994; Faure et al., 1996; Law, 1990; Tullis et al., 1973). This is in agreement with the low to moderate temperature deformation regime and greenschist facies metamorphism of the Paleoproterozoic Gangtaohe and Honghe "Group" rocks. It is noted, however, that there is an additional *c*-axis maximum consistently developed at the center of the fabric diagrams for the samples taken from the Archaean Zanhuang "Group" metamorphic rocks (99HXT-15, 99HXT-9, 99HXT-27, 99JX-32, 99JX-68, 99JX-91; Fig. 4). This probably indicates that the prismatic slip system was also active, a case for higher temperature or low-strain rate regimes. If assuming the Archaean and Paleoproterozoic rocks were subjected to similar strain rates during D_3, we can speculate that the Archaean metamorphic rocks were probably deformed under intermediate to high temperature conditions. This is consistent with the observation of amphibolite-grade metamorphism in the Archaean rocks.

In summary, all the structural and microstructural observations suggest that the D_3 event was dominated by regional extension. Uplift of the axial zone of the Zanhuang domain resulted in a divergent shearing away from the axial zone predominantly along the regional "unconformity" contact. This is consistent with top-to-WNW shearing at the western flank and top-to-ESE shearing at the eastern flank, with shearing mainly accommodated by the development of mylonitic foliations and normal faults.

3.4. D_4 deformation

D_4 deformation is represented by the development of three NNE-trending ductile shear zones (1–3 in

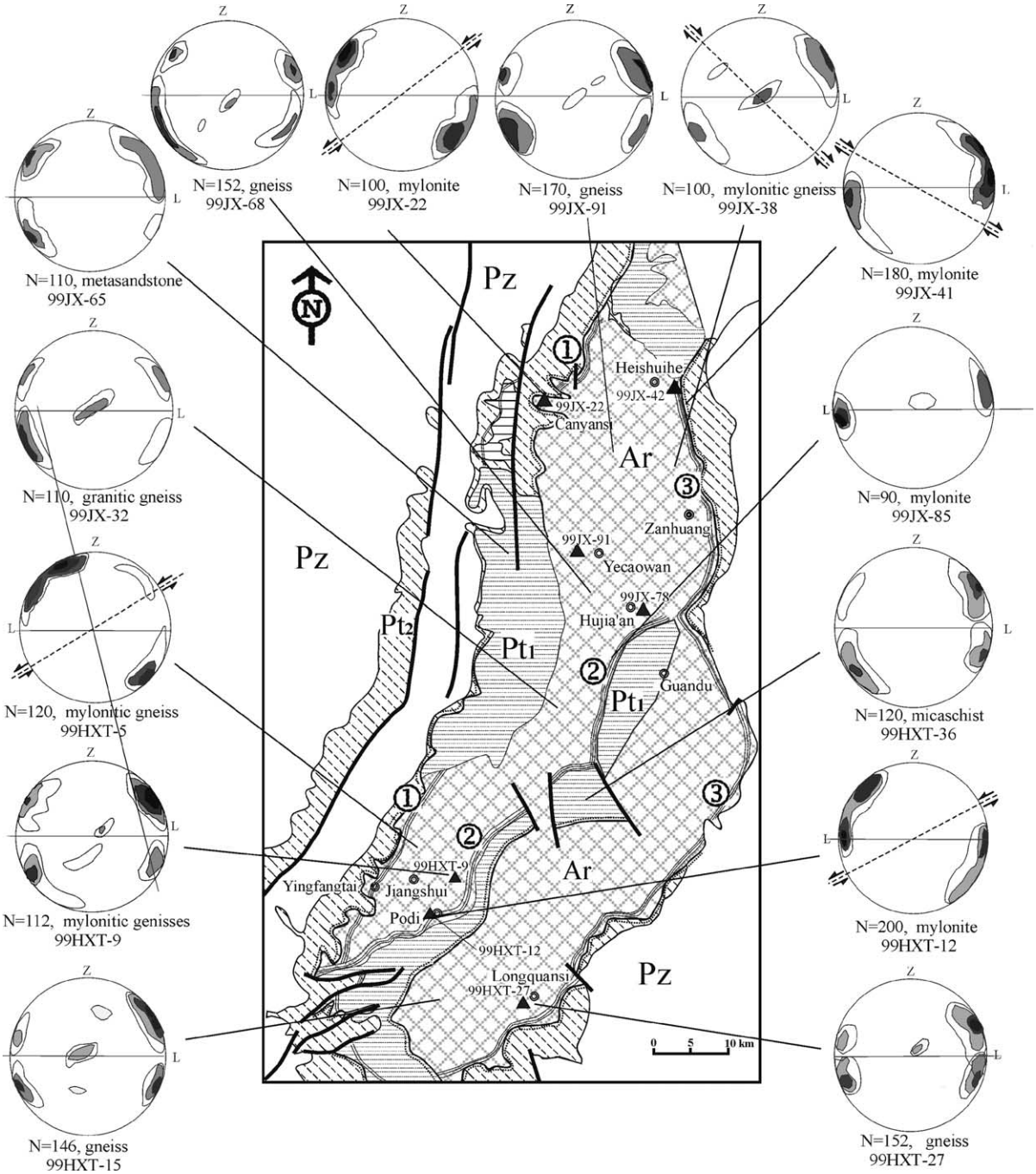

Fig. 4. Quartz *c*-axis preferred orientation patterns for metamorphic rocks and mylonites in the Zanhuang domain (L and Z give the orientations of stretching lineations and the shortening axis, respectively. Contour intervals are 1, 4, 7 and 10% (Schmidt net, lower hemisphere).

Fig. 1C; SZ_4 in Fig. 2). They are, from west to east, the Cangyansi–Yingfangtai, Podi–Haozhuang and Yudi–Heishuihe shear zones, respectively (Niu et al., 1994a,b; Lei, 1991). These shear zones displaced F_2 folds, S_2 foliations and S_3 mylonitic foliations. Some mafic enclaves derived from mafic dykes with a possible age of ca. 1700–1800 Ma (Zhai and Bian, 2000; Li et al., 2000) were deformed into lenticular structures within these shear zones. Post-S_2 folds (i.e. folded S_2 foliations during D_3) were also preserved within structural lenses in the Podi–Haozhuang shear zone.

In the three shear zones (e.g. the Podi–Haozhuang shear zone), metasedimentay rocks and gneisses were mylonitized to variable degrees from protomylonite to mylonite. S_4 mylonitic foliations are defined by a preferred alignment of muscovite, biotite and elongate quartz grains, and are strictly confined to these shear zones. The mylonitic foliations dip 15° and 45° to the WNW in the Canyansi–Yinfantai and Podi–Haozhuang shear zones, respectively, and 25° to the E in the Heishuihe–Yudi shear zone. Outcrop-scale structural lenses (Fig. 3e) and microscale S-C fabrics, mica flakes, porphyroblasts, elongated quartz grains were also well developed (Fig. 3f). These kinematic indicators indicate a top-to-W, -W and -E extensional shearing for the three shear zones from west to east, respectively (Fig. 2). This is supported by the observation of an E- or W-plunging stretching lineation (L_4) on the S_4 foliation planes and associated extensional fractures (Fig. 1C). The L_4 lineations are represented by slickenlines that were probably formed at low-moderate temperature. It was also observed in thin section that curved and kinked twins of plagioclase co-exist with microfractures. This seems to indicate that the deformation of plagioclase was in the brittle–ductile transition domain during D_4 deformation.

F_4 folds are mainly represented by drag folds developed within the three shear zones. Some normal faults of various orientations can be recognized as D_4 faults. Several of such faults crosscut unmetamorphosed mafic dykes, S_2 foliations and F_3 folds.

The quartz *c*-axis fabric diagrams derived from mylonites in the three ductile shear zones (samples 99JX-22, 99JX-41, 99HXT-12 and 99JX-85) all exhibit monoclinic point-maximum asymmetry with respect to the foliation and lineation orientation (Fig. 4). These asymmetric patterns can be used as an indication of the sense of shear along these shear zones (Bouchez et al., 1983; Law, 1990), and confirm top-to-WNW shearing along the Canyansi–Yingfangtai and Podi–Haozhuang shear zones and top-to-ESE shearing along Yudi–Heishuihe shear zone as suggested by other geometrical relationships. One sample (99JX-85) shows some *c*-axis clustering at the center of the diagram, suggesting that the prismatic slip system may also have been active and accommodated some plastic deformation (e.g. Lin et al., 2000). This pattern is in agreement with the textures derived from previous polycrystal–plasticity models and experimental studies (e.g. Tullis et al., 1973; Etchecopar, 1977; Law, 1990).

4. Mineral $^{40}Ar/^{39}Ar$ thermochronology

The $^{40}Ar/^{39}Ar$ radiometric stepwise heating method is particularly useful in deciphering a polycyclic deformation history and tectonothermal overprinting (e.g. Dalrymple and Lanphere, 1971; Hanes et al., 1988; Maluski et al., 1993; Krol and Zeitler, 1996; Holm and Dahl, 1997; Shaw et al., 1997; Reddy et al., 1997), especially in case where low-temperature events have overprinted previous high-temperature events such as in the Zanhuang domain. In this study, K-bearing minerals including biotite and K-feldspar from several mylonitic and metamorphic rocks have been selected and analyzed using this method, to provide information on the tectonothermal history of the region.

4.1. Analytical technique

All the rock samples had weathered rim removed and were crushed to millimeter-scale grains. The required minerals were carefully handpicked under a magnifier; only fresh mineral grains of 20–40 mesh grain-size were selected. A mineral purity of 99% was achieved. The selected mineral concentrates were individually wrapped in Al-foil packets, encapsulated in sealed Gd-foil, and irradiated for 2627 min at the central thimble position of the nuclear reactor (1000 kW) at the Chinese Academy of Atomic Energy Science. The instantaneous neutron flux was $6.63 \times 10^{12}\,n\,cm^{-2}\,s^{-1}$ and the integrated neutron flux was $1.05 \times 10^{18}\,n\,cm^{-2}$. The internal standard

Biotite GA1550, Biotite ZBH-25 and Amphibole BSP-1 monitors have been used, the ages of which were 97.9 ± 0.7, 132.7 ± 1.2 and 2060 ± 18.6 Ma, respectively.

The samples were progressively heated and each heating step was maintained for 20 min. Experiments were started at a temperature range of 400–430 °C and ended at 1420–1450 °C. At each extraction temperature, the impure gas released was in turn purified through a 5 Å molecular griddle, Cu–CuO (550 °C), a spongy Ti container (850 °C) and a Ti evaporated pump. Purified argon was finally collected using a Zr–Al getter pump, and subsequently analyzed using gas source mass-spectrometers operated in the static mode RGA-10 at the Institute of Geology and Geophysics, the Chinese Academy of Sciences. Measured isotopic ratios were corrected for the effects of mass discrimination and interfering isotopes (produced during irradiation), using the factors, $(^{38}Ar/^{36}Ar)_a = 0.1869$, $(^{38}Ar/^{37}Ar)_{Ca} = 3.81 \times 10^{-5}$, $(^{36}Ar/^{37}Ar)_{Ca} = 2.64 \times 10^{-4}$, $(^{39}Ar/^{37}Ar)_{Ca} = 6.87 \times 10^{-4}$, $(^{40}Ar/^{39}K)_k = 0.01$. The blank atmospheric argon $^{40}Ar/^{36}Ar$ ratio is 294.2 for this group of experiments. Total uncertainties in each apparent age (1σ) have been calculated using the methods outlined by Dalrymple and Lanphere (1971). A $^{40}Ar/^{39}Ar$ plateau of a spectrum is defined by the >60% contiguous gas fractions of all the gas evolved from the sample with invariability at 1σ level of uncertainty.

Table 2 gives the results of $^{40}Ar/^{39}Ar$ thermochronology analyses for seven biotite concentrates and three K-feldspar concentrates, and Figs. 5–7 show the age spectra (see Fig. 4 for the locations of the samples).

4.2. Biotite $^{40}Ar/^{39}Ar$ thermochronology results

Three biotite concentrates were selected from three mylonitic samples collected from the Canyansi–Yingfangtai (99JX-22), Podi–Haozhuang (99HXT-12) and Yudi–Heishuihe (99JX-41) ductile shear zones, respectively (Fig. 4). In the thin sections, plastic deformation structures such as porphyroblasts, elongated quartz grains and preferably oriented biotite flakes were observed. All three concentrates yielded variable $^{40}Ar/^{39}Ar$ spectra with similar characteristics (Fig. 5). The low- and intermediate-temperature steps

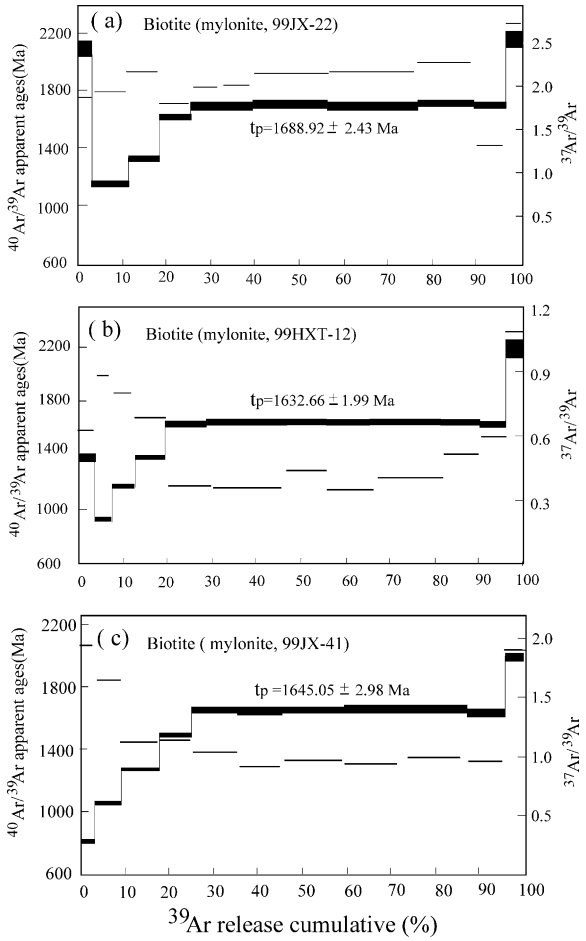

Fig. 5. The $^{40}Ar/^{39}Ar$ apparent age and $^{37}Ar/^{39}Ar$ spectra of biotite concentrates from mylonites in (a) the Cangyansi–Yingfangtai shear zone (99JX-22); (b) the Podi–Haozhuang shear zone (99HXT-12); and (c) the Yudi–Heishuihe shear zone (99JX-41). Coarse lines give the apparent ages (the length of bars reflects 1σ uncertainty), while fine lines show $^{37}Ar/^{39}Ar$ ratios. See Fig. 4 for the locations of the samples.

up to 850 °C recorded a systematic increase of apparent ages with variable $^{37}Ar/^{39}Ar$ ratios (except for the first step; see more discussion below). The plateau ages of 1688.9±2.4, 1632.7±2.0 and 1645.1±3.0 Ma are defined by intermediate- and high-temperature steps (except for the last step) over 65% gas released, which show little variations in $^{37}Ar/^{39}Ar$ ratios, respectively. The inverse ordinate intercepts ($^{40}Ar/^{36}Ar$ ratios) yielded by the $^{36}Ar/^{40}Ar$–$^{39}Ar/^{40}Ar$ isotope are close to (99HXT-12 and 99JX-22) or slightly

Table 2
$^{40}Ar/^{39}Ar$ isotopic analytical data for incremental heating experiments on biotite and K-feldspar concentrates form deformational and metamorphic rocks through the Zanhuang domain

Temp. (°C)	$(^{40}Ar/^{39}Ar)_m$	$(^{36}Ar/^{39}Ar)_m$	$(^{37}Ar/^{39}Ar)_m$	$(^{38}Ar/^{39}Ar)_m$	$^{39}Ar_k$ (10^{-12} mol)	$(^{40}Ar/^{39}Ar_k)$ ($\pm 1\ \sigma$)	$^{39}Ar_k$ (%)	Apparent age ($t \pm 1$ σMa)
Biotite concentrates from mylonite (99JX-22), weight = 0.1120 g, plateau age: 1688.92 ± 2.43 Ma								
420	286.44	0.0372	1.8833	0.0644	1.367	275.9 ± 0.04	3.51	2174.34 ± 54.28
550	119.17	0.0342	1.9788	0.0698	3.382	109.3 ± 0.00	8.69	1182.99 ± 12.69
650	137.38	0.0327	2.1462	0.0626	2.478	128.0 ± 0.01	6.36	1325.62 ± 14.79
750	159.24	0.0252	1.8052	0.0445	2.757	152.1 ± 0.01	7.08	1493.73 ± 17.93
850	189.77	0.0286	1.9872	0.0363	2.424	181.6 ± 0.01	6.22	1680.54 ± 23.76
940	186.71	0.0156	1.9838	0.0320	2.967	182.2 ± 0.01	7.62	1684.68 ± 23.25
1030	188.11	0.0139	2.1498	0.0671	6.625	184.4 ± 0.01	17.00	1697.35 ± 23.98
1100	184.67	0.0101	2.2005	0.0685	7.876	182.1 ± 0.01	20.20	1683.59 ± 23.32
1200	187.84	0.0114	2.2767	0.0655	5.049	184.9 ± 0.01	12.90	1700.33 ± 23.93
1300	192.43	0.0336	1.3072	0.0798	2.758	182.7 ± 0.01	7.08	1687.65 ± 24.84
1420	296.22	0.0943	2.6556	0.1377	1.227	269.1 ± 0.04	3.15	2142.94 ± 58.29
Inverse isochron age: 1686.00 ± 1.92 Ma, $^{40}Ar/^{36}Ar$ ratios: 303.8, MSWD: 5.6								
Biotites from mylonite (99HXT-12), weight: 0.1167 g, plateau age: 1632.66 ± 1.99 Ma								
432	217.89	0.2736	0.6096	0.1199	1.101	137.4 ± 0.002	3.32	1393.02 ± 26.99
530	126.26	0.1777	0.8774	0.0585	1.147	74.04 ± 0.00	3.45	878.39 ± 10.32
650	139.08	0.1034	0.7904	0.0436	2.017	108.7 ± 0.00	6.08	1177.90 ± 13.50
750	158.06	0.0752	0.7005	0.0440	2.156	136.0 ± 0.01	6.50	1382.78 ± 16.91
850	175.37	0.0098	0.3838	0.0325	3.061	172.5 ± 0.01	9.22	1625.05 ± 20.97
930	178.94	0.0150	0.3810	0.0296	6.169	174.5 ± 0.01	18.50	1637.68 ± 21.59
1000	177.47	0.0118	0.4578	0.0371	2.933	174.0 ± 0.01	8.84	1634.43 ± 21.39
1080	179.71	0.0181	0.3672	0.0355	3.200	174.4 ± 0.01	9.64	1636.78 ± 21.74
1160	177.72	0.0131	0.4109	0.0323	5.311	173.9 ± 0.01	16.0	1633.72 ± 21.39
1240	185.48	0.0362	0.5254	0.0370	2.875	174.8 ± 0.01	8.66	1639.61 ± 22.69
1320	189.28	0.0595	0.6032	0.0392	1.947	171.8 ± 0.01	5.87	1620.92 ± 23.18
1430	320.37	0.1111	1.1395	0.0685	1.251	287.9 ± 0.05	3.77	2228.56 ± 67.68
Inverse isochron age: 1634.19 ± 1.88 Ma, $^{40}Ar/^{36}Ar$ ratio: 280.7, MSWD: 4.8								
Biotite concentrates from mylonite (99JX-41), weight: 0.1220 g, plateau age: 1645.05 ± 2.98 Ma								
420	119.23	0.1794	1.8297	0.0974	0.903	66.62 ± 0.00	3.10	807.33 ± 10.00
530	108.44	0.0519	1.6007	0.0727	1.784	93.35 ± 0.00	6.15	1051.22 ± 11.26
650	127.77	0.0277	1.0811	0.0611	2.503	119.7 ± 0.00	8.60	1263.45 ± 13.62
750	160.65	0.0327	1.1343	0.0666	2.121	151.1 ± 0.01	7.28	1487.45 ± 18.35
850	180.07	0.0150	1.0242	0.0556	3.083	175.8 ± 0.01	10.50	1645.42 ± 22.08
930	177.04	0.0073	0.9039	0.0565	2.828	175.0 ± 0.01	9.71	1640.52 ± 21.59
1000	178.57	0.0082	0.9623	0.0532	4.219	176.3 ± 0.01	14.40	1648.38 ± 21.84
1080	179.35	0.0090	0.9207	0.0483	3.593	176.8 ± 0.01	12.30	1651.71 ± 21.93
1180	181.25	0.0130	0.9743	0.0432	4.452	177.5 ± 0.01	15.20	1655.69 ± 22.20
1280	186.23	0.0458	0.9522	0.0623	2.527	172.9 ± 0.01	8.68	1627.38 ± 22.99
1420	291.48	0.1382	1.7943	0.1425	1.089	251.2 ± 0.04	3.74	2057.46 ± 55.52
Inverse isochron age: 1650.47 ± 1.89 Ma, $^{40}Ar/^{36}Ar$ ratio: 329.6, MSWD: 11								
Biotite concentrates from gneiss (99JX-78), weight: 0.1109 g, plateau age: 1826.83 ± 0.76 Ma								
420	215.66	0.0710	1.1558	0.0951	0.962	194.9 ± 0.02	3.73	1759.26 ± 30.25
530	108.86	0.0582	0.7005	0.0537	1.831	91.80 ± 0.00	7.12	1037.87 ± 10.86
650	151.26	0.0527	2.0228	0.0730	2.282	136.0 ± 0.01	8.87	1383.10 ± 16.64
750	172.11	0.0259	1.6674	0.0750	2.410	164.7 ± 0.01	9.36	1760.23 ± 20.66
850	212.06	0.0172	1.0178	0.0655	2.689	207.1 ± 0.02	10.40	1828.38 ± 29.67
930	211.81	0.0196	1.0459	0.0531	2.944	206.2 ± 0.02	11.40	1822.97 ± 29.42
1000	209.66	0.0096	1.0060	0.0381	4.800	206.9 ± 0.02	18.60	1826.88 ± 28.87
1080	210.47	0.0133	0.9136	0.0552	2.434	206.7 ± 0.02	9.46	1825.78 ± 29.19

Table 2 (*Continued*)

Temp. (°C)	$(^{40}Ar/^{39}Ar)_m$	$(^{36}Ar/^{39}Ar)_m$	$(^{37}Ar/^{39}Ar)_m$	$(^{38}Ar/^{39}Ar)_m$	$^{39}Ar_k$ (10^{-12} mol)	$(^{40}Ar/^{39}Ar_k)$ ($\pm 1\ \sigma$)	$^{39}Ar_k$ (%)	Apparent age ($t \pm 1$ σMa)
1180	213.69	0.0238	1.0981	0.0630	1.947	206.9 ± 0.02	7.56	1826.75 ± 29.97
1300	216.66	0.0312	0.5765	0.0411	2.226	207.5 ± 0.02	8.65	1830.47 ± 30.44
1450	264.99	0.0773	0.8564	0.0657	1.198	242.4 ± 0.03	4.65	2013.85 ± 45.30
Inverse isochron age: 1822.09 ± 2.01 Ma, $^{40}Ar/^{36}Ar$ ratio = 330.5, MSWD 1.8								
Biotite concentrates within gneiss (99HXT-9), weight 0.1174 g, plateau age: 1792.61 ± 2.26 Ma								
430	111.45	0.0610	4.0614	0.1389	3.030	94.04 ± 0.01	8.55	1057.03 ± 13.21
540	117.39	0.0279	0.6425	0.0472	3.733	109.2 ± 0.00	10.50	1181.88 ± 12.23
650	149.55	0.0353	0.8501	0.0592	2.620	139.2 ± 0.01	7.39	1405.72 ± 16.40
750	197.32	0.0491	0.7257	0.0428	2.597	182.9 ± 0.01	7.32	1688.88 ± 25.22
850	204.40	0.0157	0.5527	0.0417	2.945	199.8 ± 0.02	8.31	1787.27 ± 27.46
930	205.23	0.0174	0.7303	0.0569	3.988	200.2 ± 0.02	11.20	1789.34 ± 27.79
1000	205.75	0.0132	0.8501	0.0632	5.240	202.0 ± 0.02	14.70	1799.36 ± 28.07
1080	206.38	0.0212	0.9957	0.0723	3.268	200.3 ± 0.02	9.22	1789.79 ± 28.24
1160	207.39	0.0260	0.5783	0.0339	2.666	199.8 ± 0.02	7.52	1786.96 ± 28.00
1240	211.17	0.0372	0.6682	0.0404	2.179	200.3 ± 0.02	6.15	1789.90 ± 28.86
1320	220.64	0.0580	0.7151	0.0464	1.797	203.6 ± 0.02	5.07	1808.84 ± 31.15
1450	290.67	0.1016	0.8767	0.0576	1.367	260.9 ± 0.04	3.86	2104.36 ± 54.74
Inverse isochron age: 1781.58 ± 1.98 Ma, $^{40}Ar/^{36}Ar$ ratio: 364.4, MSWD: 3.3								
Biotite concentrates from orthogneiss (99JX-91), weight: 0.1168 g, plateau age: 1719.11 ± 1.05 Ma								
420	284.84	0.1111	0.8932	0.0626	1.147	252.3 ± 0.04	2.81	1762.96 ± 52.23
540	141.23	0.0876	0.8357	0.0381	2.249	115.5 ± 0.01	5.51	1231.36 ± 14.05
650	141.88	0.0384	0.7558	0.0410	2.712	130.6 ± 0.01	6.64	1344.39 ± 15.00
750	155.85	0.0273	0.5181	0.0367	2.968	147.8 ± 0.01	7.27	1466.13 ± 17.24
830	174.28	0.0285	0.5614	0.0361	2.434	165.9 ± 0.01	6.96	1583.80 ± 20.51
900	191.13	0.0100	0.4658	0.0276	3.270	188.0 ± 0.01	8.01	1718.94 ± 24.27
980	191.34	0.0086	0.5314	0.0322	4.823	188.8 ± 0.01	11.80	1723.83 ± 24.37
1060	190.24	0.0101	0.4793	0.0280	5.705	187.3 ± 0.01	13.90	1714.65 ± 24.08
1130	191.83	0.0148	0.4377	0.0287	4.684	187.5 ± 0.01	11.40	1715.83 ± 24.87
1200	193.46	0.0196	0.5298	0.0307	3.548	187.7 ± 0.01	8.69	1717.32 ± 24.69
1270	197.74	0.0300	0.5094	0.0338	3.084	188.9 ± 0.01	7.55	1724.49 ± 25.55
1350	200.08	0.0409	0.5436	0.0319	2.829	188.1 ± 0.02	6.93	1719.28 ± 25.93
1450	320.68	0.0862	0.7623	0.0586	1.344	295.5 ± 0.05	3.29	2261.78 ± 26.84
Inverse isochron age: 1716.4 ± 1.94 Ma, $^{40}Ar/^{36}Ar$ ratio: 315.4, MSWD: 2.3								
Biotite concentrates from gneiss (99HXT-27), weight: 0.1207 g, plateau age: 1728.30 ± 0.99 Ma								
420	106.78	0.0712	0.7484	0.0519	1.606	85.63 ± 0.00	5.35	984.02 ± 10.34
540	126.53	0.0530	1.2853	0.0693	2.271	111.0 ± 0.00	7.57	1196.53 ± 13.18
650	139.37	0.0236	0.9335	0.0519	2.944	132.5 ± 0.01	9.81	1358.03 ± 15.02
750	118.09	0.0238	0.9879	0.0061	2.434	161.2 ± 0.01	8.11	1553.63 ± 19.63
830	194.69	0.0151	0.8420	0.0507	3.060	190.3 ± 0.01	10.20	1732.66 ± 25.21
900	192.57	0.0114	1.2279	0.0640	4.056	189.4 ± 0.01	13.50	1727.09 ± 24.95
980	196.38	0.0240	1.0713	0.0620	3.848	189.4 ± 0.01	12.80	1727.41 ± 25.61
1080	194.59	0.0202	1.0514	0.0655	3.431	188.8 ± 0.01	11.40	1723.48 ± 25.30
1200	197.61	0.0277	1.1173	0.0547	2.920	189.6 ± 0.01	9.73	1728.35 ± 25.75
1300	205.18	0.0518	1.0750	0.0652	2.237	190.1 ± 0.02	7.45	1731.18 ± 27.35
1420	285.43	0.1165	1.5827	0.1009	1.193	251.5 ± 0.04	3.97	2058.94 ± 52.81
Inverse isochron age: 1724.76 ± 1.94 Ma, $^{40}Ar/^{36}Ar$ ratio: 310.9, MSWD: 1.5								
K-feldspar concentrates from mylonite (99HXT-12), weight: 0.1120 g, plateau age: 1409.41 ± 0.92 Ma								
400	383.05	0.1694	1.7343	0.0949	0.683	333.6 ± 0.07	1.68	2421.09 ± 99.47
520	239.17	0.1134	1.3563	0.0804	1.124	206.0 ± 0.02	3.07	1822.21 ± 36.08
650	88.72	0.0526	0.6045	0.0315	3.084	73.28 ± 0.00	8.53	871.23 ± 8.80
750	97.86	0.0294	0.4690	0.0288	4.337	89.24 ± 0.00	11.92	1015.75 ± 10.09

Table 2 (*Continued*)

Temp. (°C)	$(^{40}Ar/^{39}Ar)_m$	$(^{36}Ar/^{39}Ar)_m$	$(^{37}Ar/^{39}Ar)_m$	$(^{38}Ar/^{39}Ar)_m$	$^{39}Ar_k$ (10^{-12} mol)	$(^{40}Ar/^{39}Ar_k)$ ($\pm 1\ \sigma$)	$^{39}Ar_k$ (%)	Apparent age ($t \pm 1$ σMa)
830	120.85	0.0184	0.4259	0.0349	3.780	115.4 ± 0.00	10.47	1230.77 ± 12.64
900	147.31	0.0268	0.3924	0.0348	3.455	139.4 ± 0.01	9.57	1407.07 ± 15.91
980	144.44	0.0146	0.4060	0.0269	7.932	140.1 ± 0.01	21.93	1412.16 ± 15.62
1060	144.69	0.0160	0.5170	0.0276	3.606	140.0 ± 0.01	9.99	1411.05 ± 15.64
1140	143.03	0.0122	0.3894	0.0274	5.659	139.4 ± 0.01	15.63	1407.05 ± 15.46
1220	143.47	0.0108	0.4766	0.0318	3.200	140.3 ± 0.01	8.87	1413.21 ± 15.57
1300	153.57	0.0491	0.7178	0.0375	2.597	139.2 ± 0.01	7.18	1405.41 ± 16.54
1450	275.51	0.1326	1.9391	0.1163	1.135	236.9 ± 0.03	2.79	1988.19 ± 48.87
Inverse isochron age: 1412.31 ± 1.71 Ma, $^{40}Ar/^{36}Ar$ ratio: 271.9, MSWD: 1.4								
K-feldspar concentrates from gneiss (99JX-78), weight: 0.2108 g, plateau age: 1423.37 ± 2.03 Ma								
420	501.75	0.3684	2.2242	0.3894	0.660	394.1 ± 0.12	1.66	2647.63 ± 179.91
530	223.02	0.0935	1.8107	0.0978	1.611	195.6 ± 0.02	4.06	1763.20 ± 31.92
640	91.75	0.0639	0.7987	0.0711	2.249	73.02 ± 0.00	5.66	868.76 ± 9.30
750	124.80	0.0426	0.3275	0.0449	2.992	112.2 ± 0.00	7.53	1205.94 ± 12.78
850	135.91	0.0316	0.3472	0.0345	3.293	126.6 ± 0.00	8.29	1314.82 ± 14.24
930	143.55	0.0122	0.2592	0.0288	3.780	139.9 ± 0.01	9.52	1410.62 ± 15.54
1000	145.11	0.0093	0.3442	0.0413	6.169	142.3 ± 0.01	15.50	1427.43 ± 15.91
1080	145.30	0.0100	0.3781	0.0412	6.911	142.3 ± 0.01	17.40	1427.41 ± 15.73
1160	144.40	0.0098	0.2085	0.0322	3.525	141.5 ± 0.01	8.88	1421.41 ± 15.72
1240	147.74	0.0193	0.3180	0.0296	3.595	142.0 ± 0.01	9.05	1425.32 ± 16.05
1320	156.35	0.0466	0.3581	0.0364	2.736	142.6 ± 0.01	6.89	1429.49 ± 17.02
1450	245.16	0.0698	0.6437	0.0419	2.156	224.7 ± 0.03	5.48	1928.06 ± 38.38
Inverse isochron age: 1418.38 ± 1.72 Ma, $^{40}Ar/^{36}Ar$ ratio: 334.9, MSWD: 7.9								
K-feldspar concentrates from gneiss (99JX-91), weight: 0.2070 g, plateau age: 1430.80 ± 2.99 Ma								
420	332.55	0.1162	1.8929	0.0860	0.996	298.8 ± 0.05	2.85	2276.32 ± 73.58
550	222.38	0.0746	2.5402	0.1164	1.551	200.9 ± 0.02	5.44	1793.45 ± 32.50
650	91.056	0.0365	1.9853	0.0682	2.849	80.53 ± 0.00	8.15	938.29 ± 9.80
715	116.79	0.0229	2.3159	0.0587	3.034	110.3 ± 0.00	8.68	1190.95 ± 12.43
850	143.18	0.0113	2.1862	0.0553	3.0557	140.1 ± 0.01	8.75	1412.21 ± 15.80
930	148.00	0.0171	2.3679	0.0645	4.053	143.3 ± 0.01	11.50	1434.12 ± 16.56
1000	145.56	0.0080	1.9692	0.0512	5.745	143.5 ± 0.01	16.40	1435.26 ± 16.13
1080	147.46	0.0126	2.2948	0.0550	3.659	144.1 ± 0.01	10.40	1439.47 ± 16.40
1160	150.33	0.0246	2.0092	0.0503	3.498	142.8 ± 0.01	10.00	1430.78 ± 16.55
1240	148.81	0.0196	2.0975	0.0338	2.942	143.3 ± 0.01	8.41	1434.27 ± 16.25
1320	189.94	0.0317	2.9755	0.0497	2.187	181.1 ± 0.01	6.26	1677.99 ± 23.90
1450	283.05	0.0847	2.8846	0.1135	1.366	258.8 ± 0.04	3.90	2094.22 ± 52.71
Inverse isochron age: 1410.06 ± 1.71 Ma, $^{40}Ar/^{36}Ar$ ratio: 361.9, MSWD: 17								

Notes: parameter $\lambda = 5.543e^{-10}/a$ and $J = 0.008471$, $(^{40}Ar/^{39}Ar)_m$: measured values of $^{40}Ar/^{39}Ar$, $^{39}Ar_k$: measured values of $^{39}Ar_k$ which was produced by k decay.

higher than (99JX-41) the $^{40}Ar/^{36}Ar$ ratio in the present-day atmosphere (295.5), an indication of no significant ^{40}Ar excess or ^{36}Ar loss, and the inverse isochron ages of the three biotites from the $^{36}Ar/^{40}Ar$ versus $^{39}Ar/^{40}Ar$ diagram are identical with their plateau ages, respectively (Table 2).

Two gneiss samples with cataphracted metacrystic texture were collected at Jiangshui (99HXT-9) and Hujia'an (99JX-78) from the axial zone of the domain (Fig. 4), respectively. The biotite concentrates derived from the samples yielded internally discordant $^{40}Ar/^{39}Ar$ age spectra. The segments for a gradual increase of apparent ages are defined by <30% of ^{39}Ar released from low- to intermediate-temperature steps, which show variable $^{37}Ar/^{39}Ar$ ratios (Fig. 6a and b). The plateau ages of 1792.6 ± 2.3 and 1826.8 ± 0.8 Ma are well defined by >70% of ^{39}Ar released during intermediate- and high-temperature

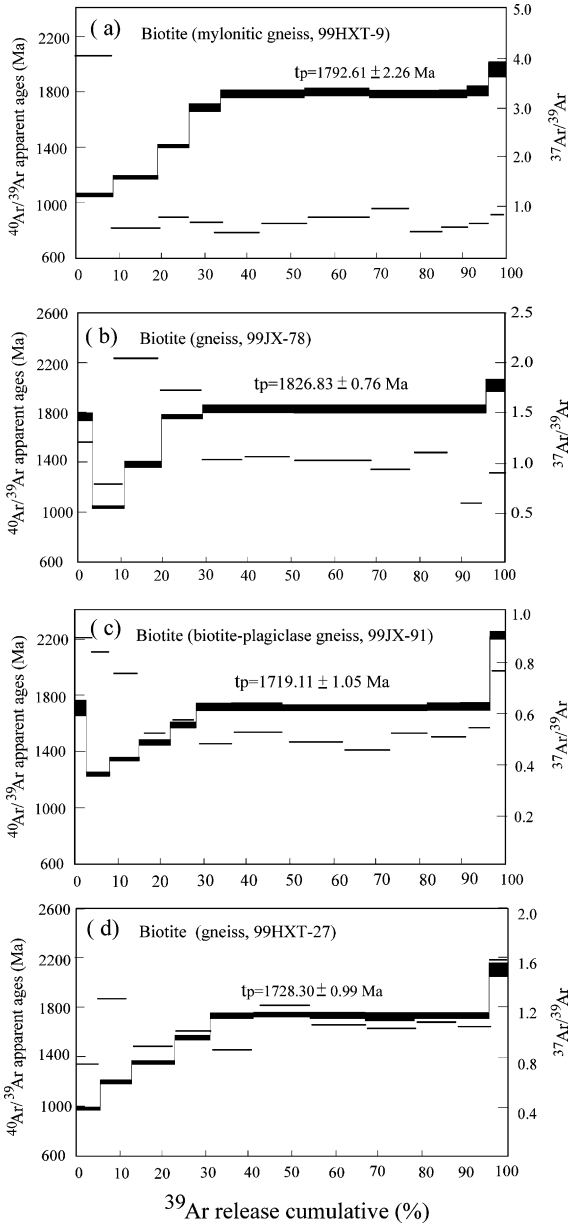

Fig. 6. The $^{40}Ar/^{39}Ar$ apparent age and $^{37}Ar/^{39}Ar$ spectra of biotite concentrates from granitic mylonite and gneiss from the axial zone (a: 99HXT-9; b: 99JX-78), eastern flank (d: 99HXT-27) and western flank (c: 99JX-91) of the Zanhuang domain. Coarse lines give the apparent ages (the length of bars reflects 1σ uncertainty), while fine lines show $^{37}Ar/^{39}Ar$ ratios. See Fig. 4 for the locations of the samples.

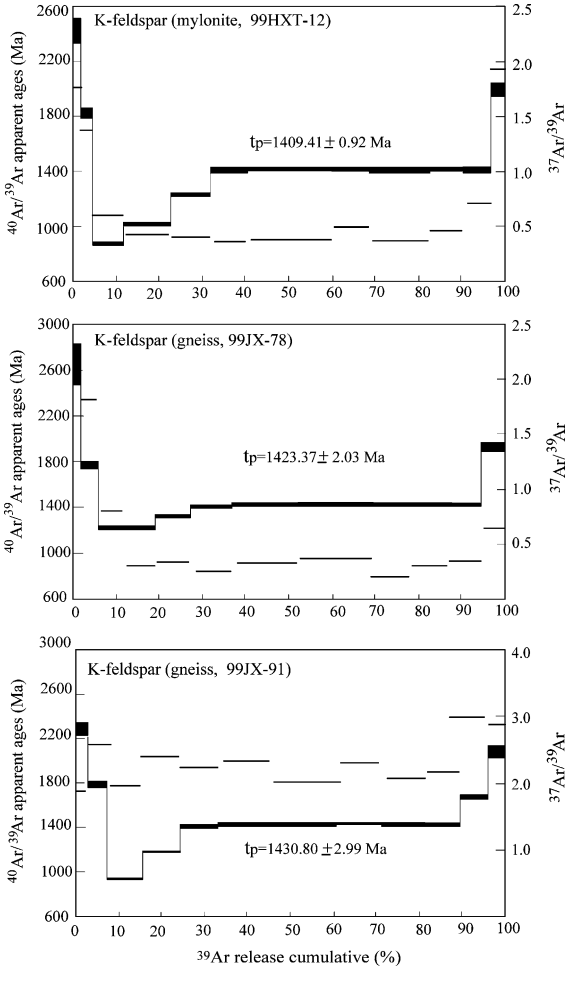

Fig. 7. The $^{40}Ar/^{39}Ar$ apparent age and $^{37}Ar/^{39}Ar$ spectra of K-feldspar concentrates from (a) mylonite (99HXT-12); (b) granitic mylonite (99JX-78); and (c) gneisses (99JX-91). Coarse lines give the apparent ages (the length of bars reflects 1σ uncertainty), while fine lines show $^{37}Ar/^{39}Ar$ ratios. See Fig. 4 for the locations of the samples.

steps with slightly variable $^{37}Ar/^{39}Ar$ ratios. The inverse isochron ages are consistent with the plateau ages, and the inverse ordinate intercepts are close to the $^{40}Ar/^{36}Ar$ ratio in the present-day atmosphere (Table 2).

Another two gneiss samples (99HXT-27, 99JX-91) were collected at Longquansi and Yecaowan, respectively (Fig. 4). Similar to the results described above, the biotite concentrates from the both samples recorded an increase of apparent ages with

variable $^{37}Ar/^{39}Ar$ ratios for low- and intermediate-temperature steps. The plateau ages of 1728.3±1.0 Ma and 1719.1±1.1 Ma were yielded for the intermediate- to high-temperature steps, respectively for the two samples, and are defined by over 70% of ^{39}Ar gas released with a relatively constant $^{37}Ar/^{40}Ar$ ratio (Fig. 6c and d). The corresponding inverse ordinate intercepts ($^{40}Ar/^{36}Ar$ ratios) are close to the value for the present-day atmosphere (Table 2).

In general, $^{40}Ar/^{39}Ar$ spectra of these biotite concentrates show a systematic increase in apparent ages with variable $^{37}Ar/^{39}Ar$ ratios for low- and intermediate-temperature increments and well-defined plateau ages with constant $^{37}Ar/^{39}Ar$ ratios for intermediate- and high-temperature increments. It is generally accepted that the ^{40}Ar in the Ca phase is first released in low temperatures and the degassing of Ca-derived Ar at low temperatures closely follows the radiogenic Ar (Foland, 1974, 1983; Fossen and Dunlap, 1998; Dallmeyer et al., 1992, 1999; Maluski et al., 1993). The $^{40}Ar/^{39}Ar$ spectra for low temperatures possibly result from: (1) a non-retentive phase with a relatively low apparent K/Ca ratio; (2) a more refractory phase with relatively low apparent K/Ca ratios; or (3) the presence of microcracks and crystalline defects induced by the development of cleavage or fractures (e.g. Maluski et al., 1993; Reddy et al., 1999). In our samples, some microcracks and the biotite crystals with minute chlorite and quartz inclusions were observed and this could lead to the degassing of Ca-derived Ar at low temperatures. Especially, an anomalous older age are occasionally observed at the lowest temperature step. This possibly resulted from the degassing of absorbent gas on mineral grain surface or of microcracks (Shuang, Institute of Geology and Geophysics, CAS, personal communication). Very similar pattern for the same minerals were also reported and the plateau ages were used to constrain the timing of deformation (e.g. Wang and Lu, 2000; Maluski et al., 1993). The well defined plateau ages of >65% of ^{39}Ar gas released at intermediate- and high-temperature should represent the mean ages obtained from the degassing of pure biotite phases (e.g. Foland, 1974). The inverse ordinate intercepts of these biotites are close to or slightly higher than the $^{40}Ar/^{36}Ar$ ratio in the present-day atmosphere and their inverse isochron ages are also identical with their plateau ages, respectively. Therefore, the plateau ages of these biotite concentrates are reliable and can be interpreted to date the timing of cooling through appropriate argon closure temperatures (300 °C, Dodson, 1973; Harrison et al., 1985; McDougall and Harrison, 1988).

The temperatures of deformation have not been precisely constrained, however, it is believed that crystal–plastic deformation becomes dominant in quartz and feldspar at the temperatures of 300 ± 50 and 450 ± 50 °C, respectively (Voll, 1976; Sibson, 1983; Kligfield et al., 1986). The lower temperature limit where quartz can be plastically deformed at geological strain rates is ca. 300 °C (Sibson, 1977; Hiroshi, 1994; Wang and Lu, 2000). As described in the preceding sections, quartz grains in the samples collected from the NNE-trending D_4 shear zones display the features of crystal–plastic deformation, while plagioclase grains exhibit the features of deformation at the brittle–ductile transition. Taking into account the dominant activation of basal ⟨a⟩ slip system in quartz during D_4, reflected in quartz *c*-axis fabric patterns for mylonites from the shear zones (see description and discussion in Section 3.4), it is likely that the D_4 deformation occurred at the temperatures of ca. 300–400 °C. Therefore, the plateau ages of 1688.9 ± 2.4 (99JX-22), 1632.7 ± 2.0 (99HXT-12) and 1645.1 ± 3.0 Ma (99JX-41) are interpreted to approximately date the cooling event through argon closure temperatures following the synkinematic growth of biotite during the mylonitic overprinting, and thus to date the D_4 ductile deformation event in the region.

The plateau ages of 1826 (99JX-78) and 1793 Ma (99HXT-9) from gneiss and mylonitic gneiss are interpreted to date the timing of post-metamorphic cooling through appropriate argon closure temperatures (ca. 300 °C) within the axial zone of the domain. Similarly, the plateau ages of 1728.3 (99HXT27) and 1719.1 Ma (99JX-91), derived from the gneisses at the two flanks of the domain are interpreted to date the timing of cooling through argon closure temperatures in these flank areas.

4.3. *K-feldspar $^{40}Ar/^{39}Ar$ thermochronology result*

Three K-feldspar concentrates were obtained from mylonites in the Podi–Haozhuang ductile shear zone (99HXT-12), gneiss in the axial zone of the domain (99JX-78) and mylonitic gneiss in the western

flank (99JX-91), respectively. The K-feldspar concentrates yielded complex ages spectra but well-defined intermediate- to high-temperature plateaus (Fig. 7). The $^{37}Ar/^{39}Ar$ ratios fluctuate at low-temperature steps in 99HXT-12 and 99JX-78, reflecting inhomogeneous phase degassing. They become more stable at intermediate- and high-temperature steps and correspond to the less affected sites during later events (Fig. 7). For the low–intermediate temperature steps, apparent ages decrease from 2647–2276 to 868–938 Ma and then increase to 1409–1430 Ma at ca. 900 °C, appearing as a depressed shape represented by ca. 25% of the ^{39}Ar gas released. Optical zonation of the K-feldspar, microcracks parallel or oblique to cleavage planes and minute chlorite inclusions are observed in thin sections. These patterns, therefore, probably result from the presence of inhomogeneous mineral phases and microcracks (Maluski et al., 1993; Dallmeyer et al., 1992, 1999; Harrison, 1990).

The plateau ages defined by over 70% of the ^{39}Ar released at intermediate- to high-temperature steps are 1409.41 ± 0.92 (99HXT-12), 1423.37 ± 2.03 (99JX-78), and 1430.80 ± 2.99 Ma (99JX-91), respectively. $^{36}Ar/^{40}Ar$ versus $^{39}Ar/^{40}Ar$ isotopic correlations from the plateau data produced inverse ordinate intercepts ($^{40}Ar/^{36}Ar$ ratios) slightly smaller or higher than the $^{40}Ar/^{36}Ar$ ratio in the present-day atmosphere (Table 2). This suggests that there is no major intracrystalline contamination with extraneous argon components (Dallmeyer et al., 1999). These plateau ages are reliable and are interpreted to date the timing of cooling through the closure temperatures of K-feldspar (ca. 160 °C, Zeitler, 1987).

5. Tectonothermal implications

The current structural analyses and mineral thermochronology study have generated new data concerning the multi-event deformation and uplift-cooling history of the Zanhuang domain during Paleo- and Meso-proterozoic.

5.1. Tectonothermal events during the Paleoproterozoic

Recent SHRIMP U–Pb dating suggests that only one phase of metamorphic zircons occurred as single grains or overgrowth rims around older magmatic zircons in both the high-grade Fuping–Hengshan gneiss complexes and the low-grade Wutai granite–greenstone terrain. These metamorphic zircons yielded consistent $^{207}Pb/^{206}Pb$ ages in the range of 1870–1800 Ma (e.g. Wilde et al., 1997, 1998; Wang and Hao, 1997; Yu et al., 1997; Wu et al., 1997; Guan, 1998; Guan et al., 2002; Zhao et al., 1998, 1999a,b, 2000, 2001; Zhao, 2001). This is also supported by the zircon U–Pb age of 1833 ± 6 Ma for garnet-bearing granites generated through the partial melting of khondalite, the Sm–Nd isochron age of 1824 Ma and the garnet $^{40}Ar/^{39}Ar$ age of 1852 Ma for high-pressure granulite in the Central Block of the North China Craton (e.g. Guo et al., 1999; Zhai and Bian, 2000; Hu et al., 1999). These data provide important support for the suggestion that the Central Block in the North China Craton resulted from collision between the Western and Eastern Blocks at ca. 1870 Ma and that there should be no major tectonic event before 1870 Ma (Zhao et al., 1999a,b, 2000, 2001; Zhao, 2001). Therefore, the earliest deformation (D_1) likely occurred at ca. 1870 Ma. The D_1 deformation is very likely to be penetrative in the Zanhuang metamorphic basement, although its structural signatures were mostly obliterated by intensive deformation during later events. Rootless and hook-like folds are the only remnant structures distinguishable in the Zanhuang domain. There are no direct geochronological constraints on the absolute timing of D_2 deformation. However, inferences can be made based on the absolute timing of D_3, discussed below.

Argon closure temperatures in biotite are inferred to be in the range of 350–300 °C for most cooling rates and chemical compositions (e.g. Harrison et al., 1985; Harrison, 1990; McDougall and Harrison, 1988). The biotite $^{40}Ar/^{39}Ar$ age of 1826–1793 Ma for metamorphic rocks, therefore, defines the timing of cooling through 350–300 °C, subsequent to the metamorphic P–T conditions (P = 6.0–7.0 kbar, T = 600–650 °C; e.g. HBGMR, 1989; Zhai, 1997; Zhao et al., 1999a,b, 2000; Zhao, 2001). This age also suggests that overprinting of younger thermal event at temperatures over 350–300 °C should be unlikely. Furthermore, the granitic pegmatite veins offsetting S_2 foliation in gneiss yielded a SHRIMP zircon U–Pb age of 1790 ± 8 Ma (Guan, 1998; Wang and Hao, 1997), and the unmetamorphosed mafic dykes in metamorphic rocks yielded a single-grain

zircon U–Pb age of 1769 Ma (Li et al., 2000) and a K–Ar age of 1790–1750 Ma (Li et al., 2000; Qian and Chen, 1987). Therefore, we speculate that the age of 1826–1793 Ma approximately confines the timing of the D_3 event in the region, and that of 1790–1780 Ma as the lower bound of the D_3 event. This is also supported by: (1) the Miaoxiangshan–Chengde-Miyun and Zhongtiaoshan–Xiong'er rifting-type magmatism in the North China Craton (ca. 1750 Ma; Gilder et al., 1991; Zhai and Bian, 2000); (2) the development of north Qilianshan embryo-ocean (ca. 1840–1780 Ma; Mao et al., 1998); (3) mafic dyke swarms within the Central Block (ca. 1700–1800 Ma; Li et al., 2000; Qian and Chen, 1987); and (4) biotite $^{40}Ar/^{39}Ar$ thermal overprinting reported for Archaean mafic granulites in Western Block and gneisses in the eastern Block of the North China Craton (ca. 1790 Ma; Wang et al., 1995; Lu and Jin, 1993). The "unconformity" between the Archaean Zanhuang "Group" and the Paleoproterozoic Gantaohe "Group", which was traditionally termed "Fuping movement" (e.g. HBGMR, 1989), thus, is not only a primary discontinuous litholigical contact but also a tectonically reworked zone (D_3 deformation) at ca. 1800 Ma (Zhao et al., 2001). Zhang et al. (1994) and Zhang (1997) also reported the presence of a 500–1000 m thick low-angle high-strain zone on the top of the crystalline basement or along the "unconformity" in the Wutai and Hengshan domains (also see Li and Qian, 1991).

The relative timing of D_2 deformation, characterized by WNW–ESE shortening and top-to-ESE thrusting, can only be logically and approximately constrained between the ages of the D_1 (ca. 1870 Ma) and D_3 (ca. 1826–1793 Ma) events. D_2 deformation probably occurred immediately following the D_1 event. It is likely that D_2 is the simple continuation of the D_1 event, driven by the crustal thickening associated with the D_1 continent–continent collision (e.g. Zhao et al., 1999a,b, 2000, 2001; Zhao, 2001) and high-grade metamorphism. This was then followed by the D_3 deformation, as a result of post-collision extensional collapse (e.g. Zhao et al., 2000, 2001; Zhao, 2001; Zhang et al., 1994; Zhang, 1997). The D_1–D_2–D_3 sequence in this region (Fig. 8a and b) seems to represent a full collision-thrusting/thickening-extensional collapse cycle (e.g. England and Thompson, 1984; Thompson and England, 1984).

The D_4 deformation occurred at 1689–1633 Ma according to the biotite $^{40}Ar/^{39}Ar$ plateau ages for the mylonites within the three NNE trending shear zones. This event was dominated by localized ductile shearing within these shear zones and is also clearly reflected by quartz *c*-axis fabric patterns. The difference of about 50 Ma between biotite $^{40}Ar/^{39}Ar$ plateau ages for the Cangyansi–Yingfangtai and for Haozhuang–Podi and Yudi–Heishuihe shear zones appears to suggest that the activation of shearing developed from west to east (Fig. 8c).

5.2. Tectonothermal uplift-cooling history since the Paleoproterozoic

Variations in the biotite $^{40}Ar/^{39}Ar$ cooling ages in the Zanhuang domain provide information about the uplift-cooling history of the region. It is noted that there is a large biotite $^{40}Ar/^{39}Ar$ cooling age difference of 70–100 Ma between the axial zone (1826–1793 Ma) and flank zones (1728–1719 Ma) of the domain. This seems to suggest a differential uplift-cooling situation for the domain. When the eastern and western flank zones cooled through the biotite $^{40}Ar/^{39}Ar$ closure temperatures (300–350 °C) at 1728–1719 Ma, the axial area where the closure temperature was reached at 1826–1793 Ma had already cooled below 300 °C. Similar to other domains in the Central Block of the North China Craton (e.g. Wutai and Fuping domains), the Zanhuang domain also encountered amphibolite-facies metamorphism described as above. Therefore, assuming that the metamorphic *P–T* conditions (5.0–7.0 kbar, 550–650 °C) for the Zanhuang domain is similar to that for other domains in the Central Block during the Paleoproterozoic overprinting (e.g. HBGMR), the cooling rates of 4.5–6.0 °C/Ma for the axial areas of the domain and 2.0–2.5 °C/Ma for the flank areas can be estimated using relevant biotite $^{40}Ar/^{39}Ar$ closure temperature. These can be approximately translated into uplifting rates of ca. 150–200 and 60–80 m/Ma for the axial and flank areas, respectively (Fig. 9), using a steady-state geothermal gradient of 30 °C/km (e.g. Hanes et al., 1988; West et al., 1993). The domain was probably finally domed by 1728–1719 Ma.

The thermal overprinting recorded by the biotite $^{40}Ar/^{39}Ar$ ages of 1689–1633 Ma only occurred within the three NNE-trending ductile shearing zones,

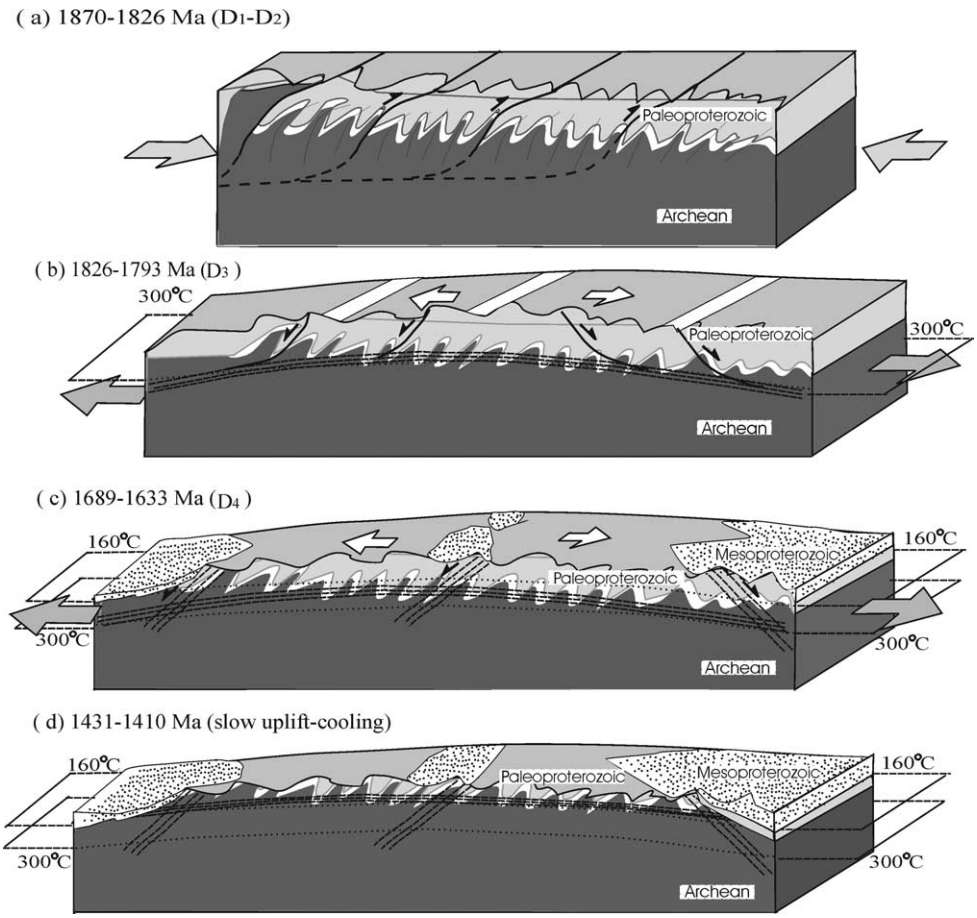

Fig. 8. Cartoons illustrating the tectonothermal development of the Zanhuang domain during the Paleo- and Meso-proterozoic. (a) 1870–1826 Ma: synmetamorphic crustal thickening and subsequent thrusting, driven by collision (D_1 followed by D_2 events). (b) 1826–1793 Ma: D_3 divergent ductile shearing deformation driven by post-collision extensional collapse. (c) 1689–1633 Ma: D_4 deformation dominated by the development of three NEE-trending ductile shear zones. (d) 1432–1410 Ma: near-horizontal isotherms cooling through 160 °C in the Zanhuang domain.

indicating that the D_4 deformation did not result in any major thermal reconstruction of the metamorphic basement on a regional scale. This also suggests that the metamorphic basement of the domain had cooled through the biotite $^{40}Ar/^{39}Ar$ closure temperature of 300 °C before the D_4 event of 1689–1633 Ma (Fig. 9). Therefore, the thermal development since 1728–1719 (the flank areas) and 1826–1793 Ma (the axial zone) can be inferred from the K-feldspar $^{40}Ar/^{39}Ar$ ages from several different tectonic locations in the domain. The similar K-feldspar $^{40}Ar/^{39}Ar$ plateau ages of 1430.8–1409.4 Ma suggest that the metamorphic basement rocks cooled to 160 °C (K-feldspar $^{40}Ar/^{39}Ar$ closure temperatures) by this time with near-horizontal isotherms having formed in the domain (Fig. 8d). The cooling rates of ca. 0.35 °C/Ma for the axial zones and ca. 0.47 °C/Ma for the flank zones can then be estimated for this period (Fig. 9). These correspond to uplifting rates of ca. 12 and 16 m/Ma for the axial and flank zones, respectively, assuming a steady-state geothermal gradient of 30 °C/km (e.g. Hanes et al., 1988; West et al., 1993).

Assuming a geothermal gradient less than 30 °C/km would lead to greater uplift rates and hence greater maximum uplift. However, it seems very unlikely that the maximum uplift in the region since ca. 1410 Ma

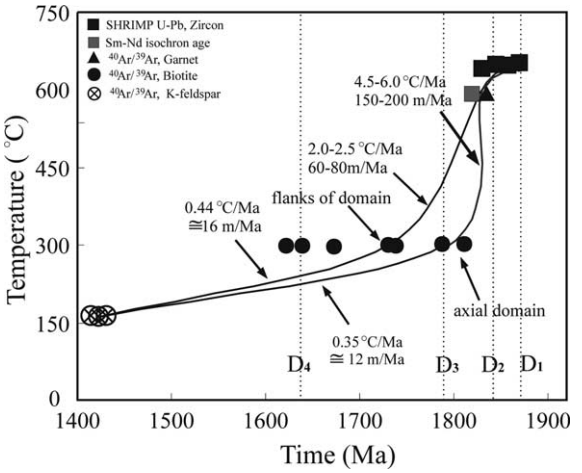

Fig. 9. Tectonothermal uplift-cooling paths of the Zanhuang domain during the Paleo- and Meso-proterozoic. Zircon SHRIMP U–Pb data are from Zhao et al. (1999a, 2001), Guan (1998) and Guan et al. (2002), and Sm–Nd isochron age and garnet $^{40}Ar/^{39}Ar$ data are from Guo et al. (1999), Zhai and Bian (2000).

can be more than 8 km, even assuming a geothermal gradient of 20 °C/km.

Collectively, the results from this study do not support the previous suggestion that the Zanhuang domain represents a Mesozoic metamorphic core complex and that it experienced rapid uplifting (>10 km) since the Mesozoic (Niu et al., 1994a,b). All the structural evidence and Mineral $^{40}Ar/^{39}Ar$ thermochronology results presented in this paper indicate that the Zanhuang metamorphic domain experienced a complex, multi-event deformation and thermal overprinting history which began during the Paleoproterozoic.

6. Conclusions

The current structural analyses and $^{40}Ar/^{39}Ar$ mineral thermochronology study demonstrate that the Zanhuang metamorphic domain is the product of a number of tectonothermal events since the Paleoproterozoic, rather than a simple "Mesozoic metamorphic core complex" as previous studies suggested. Four primary deformation events have been recognized. D_1 reflects the earliest deformation in the region and the only structures preserved include closed and rootless folds. D_2 was dominated by WNW-ESE shortening and top-to-ESE thrusting in a collisional environment. D_3 was a divergent extensional and ductile shearing event, driven by the post-collisional extensional collapse and exhumation of the thickened crust in the domain. D_4 was characterized by localized ductile shearing with the development of three NNE-trending ductile shear zones.

The $^{40}Ar/^{39}Ar$ plateau ages derived from the thermochronology analyses of biotite concentrates from the metamorphic rocks are interpreted as cooling ages through biotite $^{40}Ar/^{39}Ar$ closure temperature (300 °C) and this allows us to approximately constrain the timing of deformation events. In conjunction with the evidence from structural analyses and previous geochronological data, we conclude that 1870 and 1870–1826 Ma define the timing of D_1 and D_2 events, respectively, while 1826–1793 Ma represents the age of D_3. The last event (D_4) occurred at 1689–1633 Ma, as defined by $^{40}Ar/^{39}Ar$ plateau ages of biotite concentrates from the mylonites within the ductile shear zones. These data, together with the K-feldspar $^{40}Ar/^{39}Ar$ geochronology, also allow us to depict the cooling history of the region since post-collision extension. The estimated cooling rates are 4.5–6.0 °C/Ma in the axial areas of the domain and 2.0–2.5 °C/Ma in the flank areas during the portion of the cooling history from the peak temperature to 300 °C. Subsequent cooling through 160 °C (at 1430–1410 Ma) occurred at much slower rates. The estimated rates are ca. 0.35 °C/Ma in the axial areas and ca. 0.47 °C/Ma in the flank areas. The maximum uplift since 1430–1410 Ma in the region is less than 8 km.

Acknowledgements

We are grateful to Shefa Chen and Steve Reddy for their critical and constructive review and comments on this paper, and to Zhengxiang Li for his critical editorial comments and suggestions. We also would like to thank Peter Schaubs and Xianhua Li for their reading of the manuscript and helpful discussions and comments. This study was jointly supported by Chinese National Fund of Science grant (no. 49973021) and Chinese Academy of Science Grant (no. KZCX2-102, KZCX1-107) and Ministry of Science and Technology of China Grant (no. G1999043209).

References

Armstrong, R.L., 1982. Cordilleran metamorphic core complexes—from Arizona to Southern Canada. Ann. Rev. Earth Planet. Sci. 10, 129–154.

Bouchez, J.L., Lister, G.S., Nicoals, A., 1983. Fabric asymmetry and shear sense in movement zones. Geol. Rundsch. 72, 401–420.

Cobbold, P., Gapais, D., Means, W.D., Treagus, S.H., 1987. Shear criteria in rocks. J. Struct. Geol. 9, 1–778.

Dallmeyer, R.D., Jahansson, L., Möller, C., 1992. Chronology of Caledomian high-pressure granulite-facies metamorphism, uplift and deformation within northern parts of the Western Gneiss Region, Norway. Geol. Soc. Am. Bull. 104, 444–455.

Dallmeyer, R.D., Pana, D.I., Neubauer, F., Erdmer, P., 1999. Tectonothermal evolution of the Apuseni Mountains, Romania resolution of Variscan versus Alpine events with $^{40}Ar/^{39}Ar$ age. J. Geol. 107, 329–352.

Dalrymple, G.B., Lanphere, M.A., 1971. $^{40}Ar/^{39}Ar$ technique of K/Ar dating: a comparison with the conventional technique. Earth Planet. Sci. Lett. 12, 300–308.

Davis, G.A., Wang, C., Zheng, Y., Zhang, J., Zhang, C., Gehrels, G.E., 1998. The enigmatic Yanshan fold-and-thrust belt of northern China: new views on its intraplate contractional styles. Geology 26, 43–46.

Davis, G.A., Zheng, Y.D., Wang, C., Darby, B.J., Zhang, C.H., Gehrels, G., 2001. Mesozoic tectonic evolution of Yanshan fold and thrust belt with emphasis on Hebei and Liaoning Provinces, Northern China. In: Hendrix, M.S., Davis, G.A. (Eds.), Paleozoic and Mesozoic tectonic evolution of Central Asia: from continental assembly to intracontinental deformations, vol. 194. Geological society of American Memoir, Boulder, Colorado, pp. 171–194.

Dodson, M.H., 1973. Closure temperature in cooling geochronological and petrological systems. Contrib. Miner. Petrol. 40, 259–274.

England, P.C., Thompson, A.B., 1984. *P–T*-t paths of regional metamorphism, I. Heat transfer during the evolution of regions of thickened continental crust. J. Petrol. 25, 894–928.

Etchecopar, A., 1977. Kinematic model of progressive deformation in polycrystalline aggregate. Tectonophysics 39, 121–139.

Faure, M., Sun, Y., Sun, L., Monie, P., Charvet, J., 1996. Extensional tectonics within a subduction-type orogen: the case study of the Wugongshan dome (Jiangxi Province, SE China). Tectonophysics 263, 77–108.

Foland, K.A., 1974. ^{40}Ar diffusion in homogeneous orthoclase and an interpretation of Ar diffusion in K-fledspars. Geochimica et Cosmochmica Acta 38, 151–166.

Foland, K.A., 1983. $^{40}Ar/^{39}Ar$ incremental heating plateaus for biotite with excess argon. Isotope Geosci. 1, 3–21.

Fossen, H., Dunlap, W.J., 1998. Timing and kinematics of Caledonian thrusting and extensional collapse, Southern Norway: evidence from $^{40}Ar/^{39}Ar$ thermochronology. J. Struct. Geol. 20, 765–781.

Gilder, S.A., Keller, G.R., Luo, M., Goodell, P.C., 1991. Eastern Asia and the Western Pacific: timing and spatial distribution of rifting in China. Tectonophysics 197, 225–243.

Guan, H., 1998. Fuping Complex and its significance in Earth Precambrian crustal evolution of Sino-Korea Craton. Ph.D. Thesis, The University of Hongkong, Hongkong, pp. 32–86.

Guan, H., Sun, M., Wilde, S.A., Zhou, X.H., Zhai, M.G., 2002. SHRIMP U–Pb zircon geochronology of the Fuping Complex: implications for formation and assembly of the North China Craton. Precambrian Res. 112, 1–18.

Guo, J.H., Shi, X., Bian, A.G., Xu, R.H., Zhai, M.G., Li, Y.G., 1999. Pb isotopic composition of feldspar and U–Pb age of zircon from early Proterozoic granite in Sanggan area, North China Craton: metamorphism, crustal melting and tectono-thermal event. Acta Petrol. Sinica 15 (2), 199–207.

Hanes, J.A., Clark, S.J., Archibalo, D.A., 1988. A $^{40}Ar/^{39}Ar$ geochronological study of the Elzevir batholith and its bearing on the tectonothermal history of the Southwestern Greenville Province, Canada. Can. J. Earth Sci. 25, 1834–1845.

Harrison, T.M., 1990. Some observation of the interpretation of feldspar $^{40}Ar/^{39}Ar$ results. Isotopic Geosci. 80, 219–229.

Harrison, T.M., Duncan, I., McDougall, L., 1985. Diffusion of ^{40}Ar in biotite: temperature, pressure and compositional effects. Geochim. Cosmochim. Acta 49, 2261–2468.

HBGMR, 1989. Regional geology of Beijing, Tianjin and Heibei Province. Geology Publishing House, Beijing, pp. 50–241.

Hiroshi, Y., 1994. Kinematics of mylonitic rocks along the Median Tectonic Line, Akaishi Range, Central Japan. J. Struct. Geol. 16 (1), 61–70.

Holm, D.K., Dahl, P.S., 1997. $^{40}Ar/^{39}Ar$ evidence for Middle Proterozoic (1300–1500 Ma) slow cooling of the Southern Black Hills, South Dakota, Midcontinent North America: implications for Early Proterozoic *P–T* evolution and posttectonic magmatism. Tectonics 16 (4), 609–622.

Hu, S.L., Guo, J.H., Dai, T.M., Pu, Z.P., 1999. Continuous laser-probe $^{40}Ar/^{39}Ar$ age dating on garnet and plagioclase: constraint to metamorphism of high-pressure basic granulite from Sanggan area, North China Craton. Acta Petrol. Sinica 15 (4), 518–523.

Kligfield, R., Hunziker, J., Dallmeyer, R.D., 1986. Dating of deformation phase using K–Ar and $^{40}Ar/^{39}Ar$ techniques: results from the Northern Apennies. J. Struct. Geol. 8, 781–798.

Krol, M.A., Zeitler, P.K., 1996. Episodic unroofing of the Kohistan Batholith, Pakistan: implications from K-feldspar thermochronology. J. Geophys. Res. 101 (B12), 28149–28164.

Law, R.O., 1990. Crystallographic fabrics: a selective review of their applications to research in structural geology. In: Knipe, R.J., Rutter, E.H. (Eds.), Deformation Mechanism, Rheology and Tectonics, vol. 54. Geol. Soc. Spec. Publ., pp. 335–352.

Lei, S.H., 1991. Structural features of the Fuqingshi shear zones, Jingxing, Hebei. J. Hebei Col. Geol. 14 (3), 269–279 (in Chinese with English abstract).

Lei, S.H., Hu, S.J., 1994. Models for Fuping–Zanhuang metamorphic core complex structure, Hebei, China. J. Hebei Col. Geol. 17 (1), 54–64 (in Chinese with English abstract).

Li, J.H., Qian, X.L., 1991. A study of the Longquanguan shear zone in northern Taihang Mountains. Shanxi Geol. 6 (1), 17–29 (in Chinese).

Li, J.H., Qian, X.L., Hou, T.G., Liu, S.W., Chen, J., 2000. Late Paleoproterozoic to early Mesoproterozoic tectonic framework and major tectonothermal episodes in the North China: new

interpretation of "Luliang Orogeny". Earth Sci. 25, 15–20 (in Chinese).
Li, Z.H., 1992. On-land age of cosmic dust from Changzhougou Formation, Jixian. Geol. Rev. 38 (5), 449–456 (in Chinese).
Lin, W., Faure, M., Monie, P., Scharer, U., Zhang, L.S., Sun, Y., 2000. Tectonics of SE China: new insights from the Lushan massif (Jiangxi Province). Tectonics 19 (5), 852–871.
Lister, G.S., Davis, G.A., 1989. The origin of metamorphic core complexes and detachment faults formed during Tertiary continental extension in the northern Colorado River region, USA. J. Struct. Geol. 11, 65–94.
Liu, S.W., Liang, H.H., Zhao, G.C., Hua, Y.G., Jian, A.H., 2000. Isotopic geochronology of Precambrian Complex in Taihangshan and its geological event. Sci. Chin. (Series D) 30 (1), 18–24.
Lu, L.Z., Jin, S.Q., 1993. *P–T*-t paths and tectonic history of an early Precambrian granulite facies terrane, Jinning district, Southeastern Inner Mongolia, China. J. Metamor. Geol. 11, 483–498.
Lu, S.N., Li, H.M., 1991. U–Pb dating of single grain zircon of volcanic rocks from Dahongyu Formation in the Changcheng Group, Jixian. Bull. China Acad. Geol. Sci. (5), 111–114 (in Chinese).
Ma, W.P., He, G.Q., 1989. Late Mesozoic magmatism in the Taihang Mountains and its tectonic implication. Geol. Rev. 29 (1), 31–39.
Ma, X.Y., 1989. The geological observation in north and south of Xiangshui, Jiangsu-Madula, Neimeng geological profile. Earth Sci. 14 (1), 1–6.
Malavieille, J., 1997. Kinematics of compressional and extensional ductile shearing deformation in a metamorphic core complex of the northeastern Basin and Range. J. Struct. Geol. 19, 541–554.
Maluski, H., Rajlich, P., Matte, P., 1993. $^{40}Ar/^{39}Ar$ dating of the Inner Carpathians Variscan basement and Alpine mylonitic overprinting. Tectonophysics 223, 313–337.
Mao, J.W., Zhang, Z.C., Yang, J.M., 1998. Single-zircon dating of Precambrian strata in the west sector of the Northern Qilian Mountains and its geological significance. Chin. Sci. Bull. 43, 1289–1294.
McDougall, I., Harrison, T.M., 1988. Geochronology and thermochronology by the $^{40}Ar/^{39}Ar$ method. Clarendon Press, Oxford, pp. 1–212.
Niu, S.Y., Chen, L., Xu, C.S., 1994a. The crustal evolution and metallogenic regularity of the Taihangshan area. Seismic Publishing House, Beijing, pp. 1–203.
Niu, S.Y., Xu, C.S., Guo, L.J., 1994b. The characteristics of metamorphic core complex in Taihang Mountains and its genesis. J. Hebei Col. Geol. 17 (1), 43–52.
Qian, X.L., Chen, Y.P., 1987. Late Precambrian mafic swarms of the North China Craton. In: Halls, H.C., (Ed.), Mafic Dyke Swarms, vol. 34. Geological Association of Canada (Special Papers), pp. 385–391.
Reddy, S.M., Kelly, G.P., Magennis, L., 1997. A microstructural and laserprobe argon study of shear zone development on the western margin of the Nanga Parbat Syntaxis, Pakistan. Contrib. Miner. Petrol. 128, 16–29.
Reddy, S.M., Potts, G.J., Kelly, G.P., Arnaud, N.O., 1999. The effects of deformation-induced microstructures on intragrain $^{40}Ar/^{39}Ar$ ages in potassium feldspar. Geology 27, 363–366.
Shaw, C.A., Snee, L.W., Selverstone, J., 1997. $^{40}Ar/^{39}Ar$ thermochronology of Mesoproterozoic metamorphism in the Colorado Tront Range. J. Geol. 107, 49–61.
Sibson, R.T., 1977. Fault rocks and fault mechanisms. J. Geol. Soc. Lond. 133, 191–213.
Sibson, R.H., 1983. Continental fault structure and the shallow earthquakes source. J. Geol. Soc. Lond. 140, 741–767.
Simpson, C., Schmid, S., 1983. An evalution of criteria to deduce the sense of movement in sheared rocks. Geol. Soc. Am. Bull. 94, 1281–1288.
Tang, X.M., Liu, S.W., 1997. An initial research on the extension deformation belt in the Archean metamorphic rocks in the Northern Taihang Mountains. Acta Scientiarum Naturalium Universtatis Pekinensis 33 (4), 447–455.
Thompson, A.B., England, P.C., 1984. *P–T*-t paths of regional metamorphism, II. Their influences and interpretation using mineral assemblages in metamorphic rocks. J. Petrol. 25, 929–950.
Tullis, J., Christie, J.M., Griggs, D.T., 1973. Microstructure and preferred orientations of experimentally deformed quartzites. Geol. Soc. Am. Bull. 84, 297–314.
Twiss, R.J., Moores, E.M., 1994. Structural geology. W.H.Freeman and Company, New York, pp. 215–422.
Voll, G., 1976. Recrystallization of quartz, biotite and feldspar from the Erstfeld to the Leventina nappe, Swiss Alps and its geological significance. Schweizerische Mineralogische and Petrographische Mitteilungen 56, 641–647.
Wang, K.Y., Hao, J., 1997. SHRIMP dating of single grain zircon and its constraints on the Wutai orogenic event. Chin. Sci. Bull. 42 (1), 1295–1298.
Wang, S.S., Sang, H.Q., Qiu, J., 1995. Metamorphic age of metamorphic rocks underlain by the Changcheng Group and its constraints on the lower-limit age of the Changcheng Group in Tianjing area. Geol. Sci. Sinica 30 (4), 348–354 (in Chinese with English abstract).
Wang, Z.H., Lu, H.F., 2000. Ductile deformation and $^{40}Ar/^{39}Ar$ dating of Changle-Nan'ao ductile shear zone, southeastern China. J. Struct. Geol. 22, 561–570.
West, D.P., Lux, D.R., Hussey, A.M., 1993. Contrasting thermal histories across the Flying Point fault, southwestern Maine: evidence for Mesozoic displacement. Geol. Soc. Am. Bull. 105, 1478–1490.
Wilde, S.A., Cawood, P.A., Wang, K.Y., 1997. The relationship and timing of granotoid evolution with respect to felsic volcanism in the Wutai Complex, North China Craton. In: Proceedings of the 30th IGC on Precambrian Geol. Metamorph. Petrol., vol. 17, pp. 75–88.
Wilde, S.A., Cawood, P.A., Wang, K.Y., 1998. SHRIMP U–Pb data of granites and gneisses in the Taihangshan–Wutaishan area: implications for the timing of crustal growth in the North China Craton. Chin. Sci. Bull. 43, 144.
Wu, C.H., Zhong, C.T., Chen, Q.A., 1997. Ages of khonodalites in the Jin–Ji–Men high-grade terrains, North China Craton. Acta Petrol. Sin. 13, 28–50 (in Chinese).
Xu, R.H., Zhu, M., Chen, F.K., Guo, J.H., 1995. A geochronological study of the Longquanguan ductile shear zone. Quaternary Sci. 4, 332–342.

Yu, J.H., Wang, D.C., Wang, X.Y., Li, H.M., 1997. Age of the Luliang Group and its main metamorphism in the Luliang Mountains, Shanxi: evidence from single grain zircon U–Pb ages. Geol. Rev. 43 (4), 403–408 (in Chinese with English abstract).

Zeitler, P.K., 1987. Argon diffusion in partically outgassed alkali feldspar: insights from $^{40}Ar/^{39}Ar$ analysis. Chem. Geol. 65, 167–181.

Zhai, M.G., 1997. Recent advance in the study of granulites from the North China Craton. Int. Geol. Rev. 39, 325–341.

Zhai, M.G., Bian, A.G., 2000. Ultracontinental collision at the end of Neoarchean and its breakup between end of Paleoproterozoic and Mesoproterozoic in North China Craton. Science in China (series D) (Supplement), 129–131 (in Chinese).

Zhang, J.S., 1997. Extension and uplift of the Datong–Huai'an granulite terrain. Geol. Rev. 43 (5), 503–514.

Zhang, J.S., Dirks, P.H., Passchier, C.W., 1994. Extension collapse and uplift in a polymetamorphic granulite terrian in the Archean and Paleoproterozoic of North China. Precambrian Res. 67, 37–57.

Zhang, S.G., Jin, L.G., Xiao, Q.H., 1983. The structural style of Fuping Archean dome-complex fold and its deformational history. Chin. Regional Geol. 6, 1–12 (in Chinese with English abstract).

Zhao, G.C., 2001. Paleoproterozoic assembly of the North China Craton. Geol. Mag. 138 (1), 89–91.

Zhao, G.C., Cawood, P.A., Lu, L.Z., 1999a. Petrology and *P–T* history of the Wutai amphibolites: implications for tectonic evolution of the Wutai Complex, China. Precambrian Res. 93, 181–199.

Zhao, G.C., Cawood, P.A., Wilde, S.M., Sun, M., Lu, L.Z., 2000. Metamorphism of basement rocks in the Central zone of the North China Craton: implications for Paleoproterozoic tectonic evolution. Precambrian Res. 103, 55–88.

Zhao, G.C., Wilde, S.A., Cawood, P.A., Lu, L.Z., 1998. Thermal evolution of Archean basement rocks from the eastern part of the North China Craton and its bearing on tectonic setting. Inter. Geol. Rev. 40, 706–721.

Zhao, G.C., Wilde, S.A., Cawood, P.A., Lu, L.Z., 1999b. Tecono-thermal history of the basement rocks in the western zone of the North China Craton and its tectonic implications. Tectonophysics 310, 223–240.

Zhao, G.C., Wilde, S.A., Cawood, P.A., Sun, M., 2001. Archean blocks and their boundaries in the North China Craton: lithological, geochemical, structural and *P–T* path constraints and tectonic evolution. Precambrian Res. 107, 45–73.

Zhao, T.P., Zhou, M.F., Jin, C.W., Guan, H., Li, H.M., 2001. The formational age of Xiong'er Group in southern North China Craton. Chin. J. Geol. 36 (3), 326–334.

Zheng, Y.Z., Zhang, Q., Wang, Y., Liu, R., Wang, S.G., Zuo, G., Wang, S.Z., Lkaasuren, B., Badarch, G., Badamgarav, Z., 1996. Great Jurassic thrust sheets in Beishan (North Mountains)–Gobi area of China and southern Monogolia. J. Struct. Geol. 18, 1111–1126.